

See discussions, stats, and author profiles for this publication at: <https://www.researchgate.net/publication/347949769>

Overview on the development and critical issues of water jet guided laser machining technology

Article in Optics & Laser Technology · May 2021

DOI: 10.1016/j.optlastec.2020.106820

CITATIONS

5

READS

1,232

5 authors, including:



Yan Liu

Huazhong University of Science and Technology

40 PUBLICATIONS 31 CITATIONS

[SEE PROFILE](#)



Meirong Wei

Huazhong University of Science and Technology

6 PUBLICATIONS 8 CITATIONS

[SEE PROFILE](#)



Tao Zhang

Huazhong University of Science and Technology

56 PUBLICATIONS 465 CITATIONS

[SEE PROFILE](#)



Hui Li

Wuhan University

117 PUBLICATIONS 934 CITATIONS

[SEE PROFILE](#)

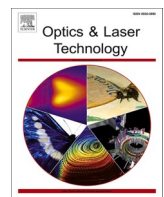
Some of the authors of this publication are also working on these related projects:



(1) Simulation of the fluid performance of super large storage hard disk drive [View project](#)



(4) Intelligent manufacturing of electronic products based on process modeling and simulation [View project](#)



Review

Overview on the development and critical issues of water jet guided laser machining technology

Yan Liu ^{a,d}, Meirong Wei ^a, Tao Zhang ^{a,d,*}, Hongchao Qiao ^{b,*}, Hui Li ^c^a School of Naval Architecture and Ocean Engineering, Huazhong University of Science and Technology, 430074, PR China^b Shenyang Institute of Automation Chinese Academy of Science, Shenyang 110016, PR China^c School of Power and Mechanical Engineering, Wuhan University, 430072, PR China^d Hubei Key Laboratory of Naval Architecture and Ocean Engineering Hydrodynamics, 430074, PR China

ARTICLE INFO

ABSTRACT

Keywords:

Waterjet guided laser
Multiphase fluid dynamics
Laser-fiber coupling
Laser-matter interaction
Laser material processing

There was no established literature or documentation regarding this due to the competition for the market and confidentiality issues. This article reviews the current status of waterjet guided laser (WJGL) processing. This paper addresses the state-of-the-art development and knowledge in WJGL technology. The paper attempts to support researchers as well as practical engineers who are considering this non-traditional manufacturing method for application in their field.

The topic is developed following the history of the water-jet guided laser technology. It outlines the primary aspects of industrial use, their relevant applications, and the variety of laser beam sources available. Here the principle, machine configuration and benefits of the WJGL technology are elaborated. The formation process of water jet, optical characteristics of water, the influence of different factors on the stability of jet are discussed. In this paper different aspect of laser-waterjet coupling like coupling unit, parameters, loss, propagation modes and speckle etc. are discussed. The major factors which affect transmission efficiency are wavelength of laser, focal position and numerical aperture. After giving some more details on the operating principle and its realization, the following sections WJGL-matter interaction, modeling of material removal, laser induced bubble and breakdown are presented. In this paper an attempt is made to present a literature survey on waterjet guided laser technology.

1. Introduction

Water is one of the most common transparent materials on earth. The idea of using water as an optical element is as old as the optical sciences themselves. Guiding light rays with water jet was observed by Prof. Daniel Colladon in 1841 [1]. Instead of traveling in a straight line, the light followed the curve of a non-turbulent stream of water. (The possibility of guided light in water-jet was first demonstrated by a French physicist Jacques Babinet and his Swiss counterpart Jean-Daniel Colladon in the 1840 s.) In 1854, Tyndall successfully demonstrated the flow of water jets and how total internal reflection could guide the light along the flowing liquid by following the suggestion of his mentor, Faraday. Water jet became indeed the first optical fiber [2]. The first a pulsed ruby laser was invented and tested in 1960 [3]. Thereafter, laser became a widely used efficient source of light for commercial and industrial application due to its excellent properties of spatial and temporal

coherence. Elias Snitzer of American Optical demonstrated a laser directed through a thin glass fiber that had implications in medicine in 1961 [4]. In 1965, the first production laser cutting machine was used to drill holes in diamond dies [5]. Since then, laser irradiation is used in a variety of ways for the material processing in the industry, such as cutting, drilling, welding, marking, etc. For nearly all of these methods, the laser beam is focused with the aid of an optical element on the material to be processed in order to generate the enough intensity necessary for the processing operation. In 1985, Yuauru Doi in Asahi K.K. (Tokyo Japan) tried to fuse water with laser by inventing a laser knife which supplies water to a rod member applying laser radiation to tissue [6]. Walter-Gerhard Wrobel in Aesculap AG improved the design by adjoining a compact liquid jet of laser-radiation-transmissive with a solid light guide core, which guided a laser beam to a workpiece, in 1986 [7]. In 1991, B. Richerzhagen, E. Leiglon, etc. in LASAG refined this principle by generating the liquid column using a waterjet nozzle and

* Corresponding authors.

E-mail addresses: zhangt7666@hust.edu.cn (T. Zhang), hcqiao@sia.cn (H. Qiao).

focusing the laser into the nozzle inlet [8]. The light guiding water jet in its modern form, the water jet-guided laser, was realized in the framework of a project for laser dentistry in 1993 [9]. B. Richerzhagen made a further refinement step at École Polytechnique Fédérale de Lausanne, Switzerland, in 1994 based on the same principle [10] and, then, commercialized by Synova (Lausanne, Switzerland) in 1997, transforming the improvements into the process known as Water Jet Guided Laser (WJGL). In 2004, A. Kruusing investigated underwater and water-assisted laser processing, such as steam cleaning and shock processing [11,12]. At present, more and more companies, such as Avonysis, Sugino Corp, Shibuya Corp, start to provide WJGL machines to the market [13–15]. However, the research work is still limited in the field. In this paper, the development of a WJGL machine and some critical issues are reviewed.

2. Water jet guided laser technology

The water-jet laser cutting technology has many advantages over conventional lasers, because it combines the advantages of water jet and laser. The original idea of WJGL technology was invented to suppress the pain by cooling the tooth in laser dentistry. However, the use of a waterjet instead of an assist gas stream, which is widely employed in conventional dry laser cutting, eliminates a lot of problems associated with dry laser and demonstrates versatile and superior machining ability. In consequence, a wide array of materials either ultra-hard, brittle, or heat and mechanically sensitive, either conductive or isolating materials can be processed as long as the laser wavelength selected can be absorbed by the materials [16–21].

Compared to dry laser cutting, With WJGL, much of the energy dissipates into the water and not in the material. The water jet cools the edges of the cut and its immediate surrounding area between laser pulses, reducing heat-affected zone (HAZ) and thermal residual stress and preventing heat damage within the materials. Focal optics of WJGL technology are not required. The focused spot diameter varies along the axis of the laser beam. Once laser beam being funneled into a waterjet, no complicated and expensive real-time focus control and tracking system is required. High precision, high quality ablation and cutting edges can be implemented with WJGL. Thanks to a much higher kinetic energy density than any assist gas flow used in dry laser cutting, water jet can expel the molten material from the cut more efficiently. The expulsion and the cooling enable the ablation to generate kerfs with very smooth walls, free of deposition, burr and cavities on the edge. The total

resulting mechanical forces exerted on the workpiece is negligible and WJGL processing can be considered as contactless and is not subject to mechanical stress and wear. Finally, WJGL does not require electrical conductivity, therefore, a wide range of metal and non-metal materials can be machined. Additionally, WJGL lower the air dust by absorbing the cutting waste with water. The ablation products are bound to the water and no hazardous materials are released to the atmosphere.

2.1. Operating principle

Laser ablation is the process of removing material from a solid surface by irradiating it with a pulsed or continuous wave high power laser beam. At low power intensity, the material is heated by the absorbed laser energy, resulting in melting, vaporization or sublimates. At high power intensity, the material can be converted to a plasma. The concentrated light results in an intense heat input locally, bringing about unwanted thermal side effects, such as surface contaminations, heat-affected zones, burrs and micro-cracks. In a conventional dry laser cutting, assistant gasses are required to remove the molten debris and obtain the required quality of cut. WJGL ablates the materials in a similar way, but with a totally different strategy to avoid the weaknesses dry laser induced. A lot of laser induced troubles are prevented intrinsically.

The operating principle of WJGL technology is illustrated in Fig. 1. High power laser energy is funneled and propagated to the workpiece through a capillary laminar water jet column, rather than focusing the laser beam on the workpiece directly. Once the waterjet in the stable range collides with the workpiece, the guided laser power is dispersed and absorbed by the material. Resulting heat melts and vaporizes the ablation zone.

A basic WJGL supporting system mainly consists of four units as shown in Fig. 2, namely, the laser and optics unit, the water supply unit, the shielding gas unit, and the coupling head unit.

Medium pressure water ranging from 5 to 80 MPa is forced through an orifice in a compressed water filled chamber to create a capillary laminar water jet which works as a hair thin optical fiber with variable length. The diameters of the orifice range from 10 to 200 μm . The nozzles mounted at the exit of a water chamber are made of sapphire, ruby or diamond to resist the wear. The level of water consumption is in the order of 1 L/hour at 30 MPa. Degassed ultra-pure water is provided due to the high requirements of water quality. Beside of transmitting laser energy, the jet simultaneously takes care of cooling and cleaning. A

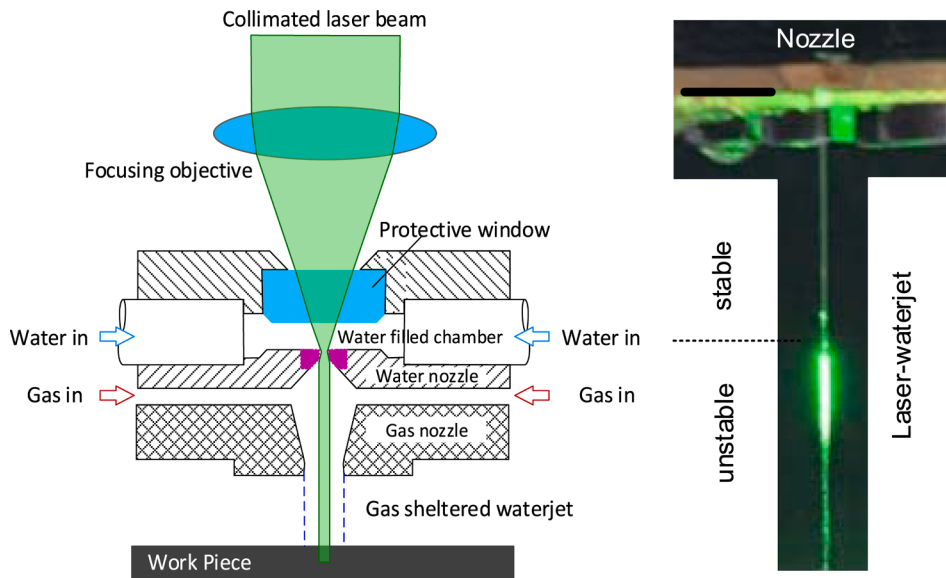


Fig. 1. Operating principle of waterjet guided laser technology (revised from [22]).

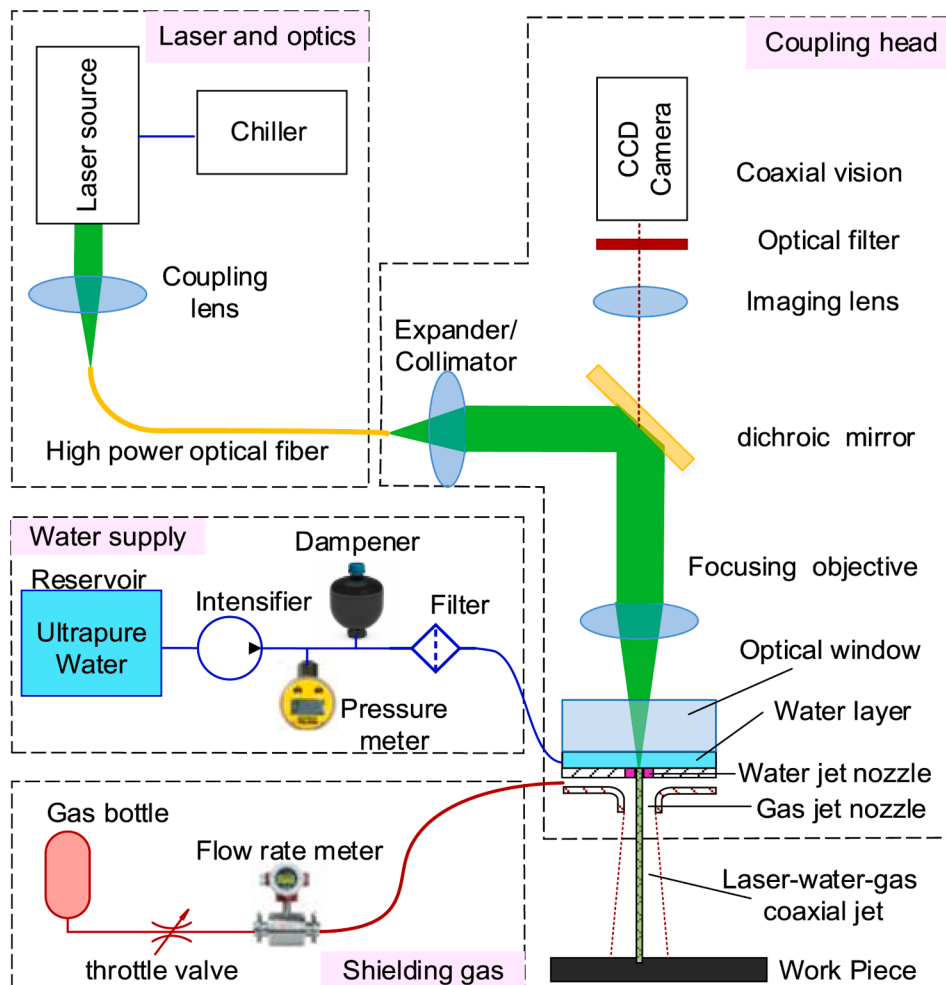


Fig. 2. Sketch illustrating a WJGL supporting system.

transparent optical window is embedded at the top of the water chamber to allow laser light transmission. Coaxial shielding gas stream is applied to surround the waterjet stream in order to decrease the disturbance from the ambient atmosphere and enhance the coherent length of the waterjet.

A wide range of laser sources are available commercially for WJGL, including pulsed diode pumped solid state (DPSS) laser, fiber laser, disk laser, which operates at 1064, 532 or 355 nm. The laser source is always chosen carefully depending on the application and the cutting requirements. Usually ns-pulsed lasers are chosen in the range of 1–500 ns. The WJGL can be used for a wide range of material ablation, only limited by insufficient material absorption of the laser light (glass, wood, tissues) or high reflectivity (copper).

In the coupling head, the laser which diverges from the glass optical fiber is collimated/expanded and reflected through a series of lenses and mirrors and then focused precisely on the center of the nozzle aperture which is generating the water jet. Dichroic mirror allows the laser beam to be bent. Meanwhile, the focusing vision image is allowed to pass through to the CCD camera. Leaving the nozzle, the laser beam is guided inside the water jet in the manner of total internal reflection at the water-air interface. Laser beam is guided over the entire, exceptionally long and perfectly cylindrical working distance to the surface of the workpiece [23–25].

2.2. Machine configuration

A typical water jet guided laser machine mainly comprises of a

pressure water and shielding gas supply Sub-system, laser and cooling Sub-system, a CNC motion platform, and waterjet-gas-laser coupling head as shown in Fig. 3.

The water supply system consists of a high-pressure water pump and ultrapure water treatment. The pump is designed to deliver a pulsation-free stream of water to the coupling assembly of the laser head with an output pressure up to 800 bar. Shielding gas is supplied by a gas bottle with its flowrate adjusted by a flowrate meter [26].

The coupling head, the central element enabling the coupling of the laser beam to the laminar water jet, consists of laser beam-delivery optics, a high-resolution alignment and focusing motion system, a laser-waterjet-gas coupling assembly, a vision and illumination system. The focusing objective are designed for on-axis high power laser focusing and micro-image alignment vision simultaneously [27].

The workpieces fixed on a motorized stage are moved under the water-jet guided laser beam during the cutting process. The motion of coupling head in the perpendicular direction is only necessary in order to adapt to the different working distances of differently sized nozzles at different water pressures. Normally the coupling head should be positioned vertically in case the waterjet may be bent by the gravity too much, leading the laser power escaping from the waterjet. The work-piece can be tilted mechanically to give angled cutting. The precision achieved is a function of the precision of the motion system, the diameter of the nozzle aperture and the process parameters applied.

The operation of the sub-systems is controlled by PC and PLC separately and coordinated through industrial Ethernet. Safety aspects for the WJGL machine is set properly with interlocked mechanisms. The

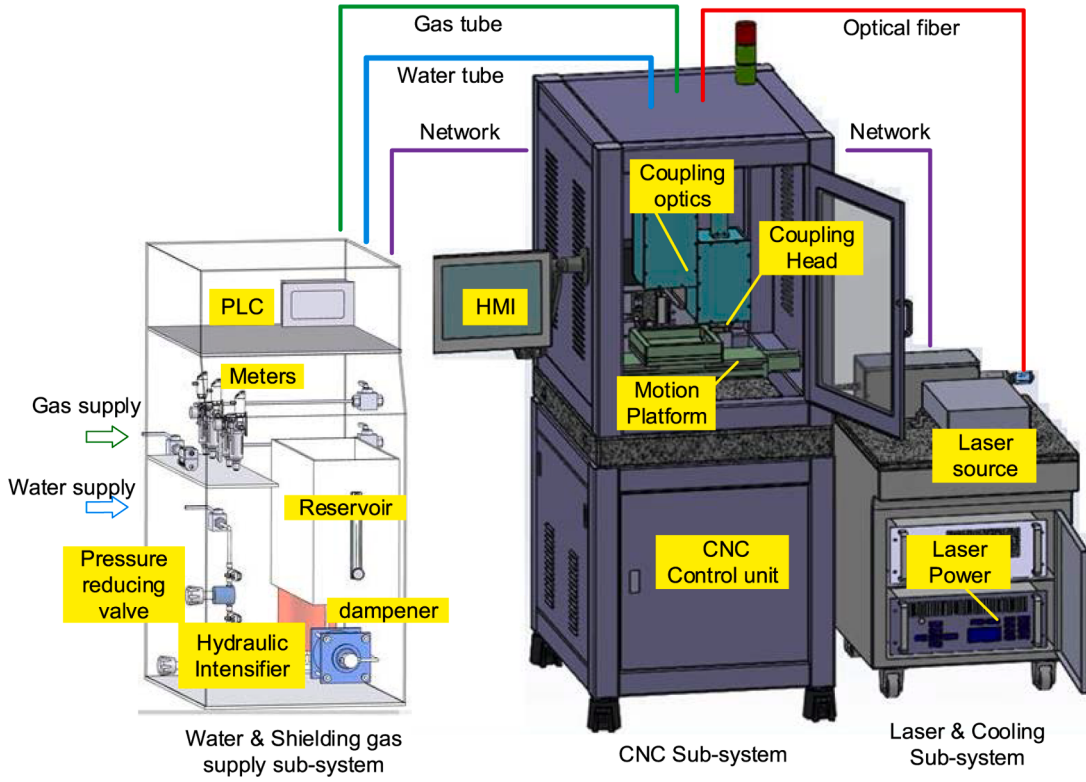


Fig. 3. The main sub-systems of a WJGL machine.

laser is switched off automatically if the water pressure and level drops below a certain value to avoid the dry laser damaging the nozzle. The door must be closed before the machine be operated to avoid laser injure [28].

2.3. Ablation process

A typical water jet guided laser ablation cycle are illustrated as shown in Fig. 4 [29–33].

Initially, a waterjet is generated and directed onto the workpiece without laser energy. A stable waterjet fiber formed. A water film formed by impinging force spreads on the surface of workpiece.

- (a) Laser power switches on and a laser pulse is released and guided by the waterjet fiber to the surface of the workpiece. On hitting the workpiece, the laser energy is efficiently transferred to the material being processed. Laser power is absorbed by the material and heats the target area.
- (b) As the heat accumulates at the local processing area, the material is molten and vaporized. At low laser flux, the material is heated by the absorbed laser energy and evaporates or sublimates. At high laser flux, the material is typically converted to a plasma. The absorbed laser energy generates a vapor or plasma on the surface which separates the water jet and the workpiece. Water jet is lifted off. Shockwave is generated and recoil pressure of vapor and expanding plasma expel the melt out, preventing material recast at the cutting edge. The water film works as the

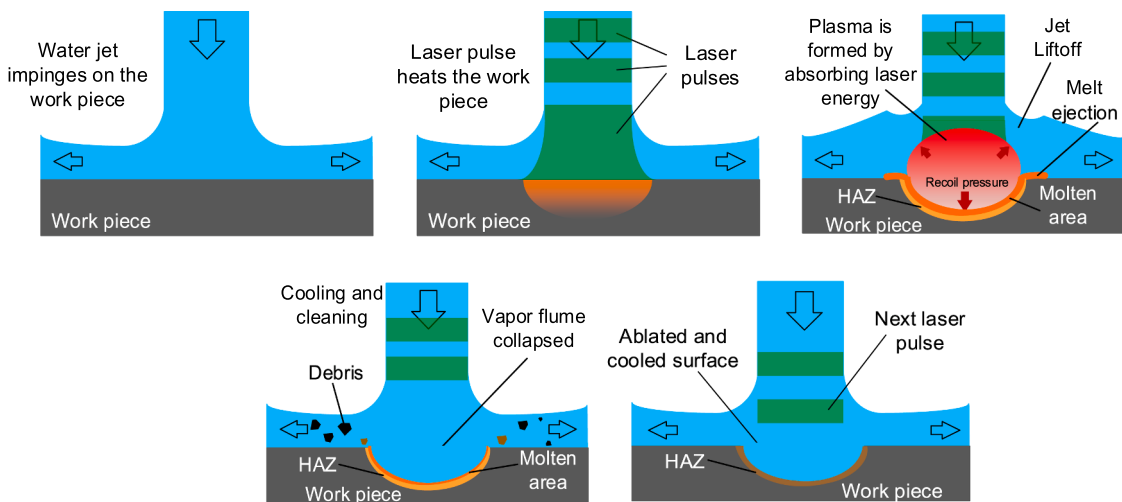


Fig. 4. A typical water jet guided laser ablation cycle.

confinement layer to redirect the shockwave towards the processing material and improve the laser ablation efficiently since the pressure caused by shockwave in the water film is much larger than that in the air. Hot particles are pushed back by the water jet.

- (c) At the end of each laser pulse, the vapor plume collapses and the plasma disappears. The water jet expels the molten material and cools the ablation zone to water temperature. Local heat accumulation due to the multiple pulses and thermal expansion are reduced. Debris is flushed away by the water flow and burr formation is prevented. This laser ablation round is completed.
- (d) Then the next laser pulse reaches. A new cycle of the ablation process starts again. The whole process experiences continuous alternation of heating and cooling as shown in Fig. 5. The ratio between the duration of laser pulses and the interval time between the pulses can be tuned to optimize the machining speed and the material cooling effects.

3. Hydrodynamic issues

3.1. Flow regions

To guide laser energy to a workpiece, compressed water issues from a small orifice to form a capillary optical waterjet fiber. There exist four flow regions for a waterjet optical fiber as shown in Fig. 6 to be ejected, extend, and eventually impinge on the workpiece: flow in a compressed water chamber, jet generation, free jet, and impinging jet. The water arrives in the chamber from all directions with no turbulences existing in the process. Different from a plastic or glass optical fiber, the waterjet optical fiber is too weak to be disturbed and breakup. Breakup of fluids can be described as the procedure when bulk liquid disintegrates into droplets by the action of both internal and external forces. Water properties, temperature, turbulence, particles and bubbles in the water, and ambient environment affect the stability of the waterjet apparently. The length of the free jet part limits the working distance within which the water jet has a stable, constant diameter and laser power can be propagated efficiently. The laser spot transmitted also presents a constant round shape in this range. On the material, stagnation point of the impinging water jet leads to widening of the water jet. Beyond the working distance, the waterjet is ruffled and no longer keeps a cylindrical shape. The pressure of the jet decreases. Even still in the coherent length, the laser beam leaves the water jet in a diffusive manner, forming a brilliant segment along the waterjet. Eventually, the jet is disrupted and atomized. Thus, hydrodynamic stability is one governing factor in forming the capillary optical waterjet fiber and limits the laser ablation.

The free jet region of a waterjet optical fiber, the major part of a waterjet optical fiber, can be classified into a step-index fiber as the core of a waterjet which has a uniform index refraction is surrounded by an atmosphere cladding. In order to transmit the laser power efficiently, the shape of the waterjet is close to a cylinder with smooth interface between water and atmosphere for total internal reflection. The water flow and waterjet should present laminar status and free of bubbles and

particles to increase uniform light waveguide path. Longer stable length is desired to create more working space and enable deeper machining ability. Finer diameter is also preferred for high accuracy and precision machining. It's better to keep a waterjet vertical and away from electric fields since gravity and electric fields can bend the waterjet optical fiber.

The compressed water supply system as shown in Fig. 7 is designed to deliver a stream of water to the laser-waterjet coupling head that depending on pump configuration can have an output pressure of up to 800 bar. A pressure reducing valve to adjust the output pressure. The water pressure depends on the orifice diameter. Larger nozzle diameters require a smaller water pressure. For precise applications, smaller diameters are desirable. Surge and pulsation problems which affect the stability of a waterjet are fairly common in the fluid power arena. Hydraulic intensifiers or pumps with multiple hydraulically driven pistons are good options. Rotational pumps are not suitable due to the pulsation of these kind pump. Surge suppressors can be installed near the pump outlet, or near the inlet of shut-off valves. The pressure fluctuations can also be decreased using a nitrogen loaded accumulator. Algorithms can also be programmed to control the pressure and make the fluctuation smooth.

WJGL machining is very sensitive to the water quality. Particles in the water not only block the orifice, but also disturb the laminar water flow. Dust particles in the area with high power density can be melted and vaporized, rendering turbulence and waterjet breakup. Particles also deteriorate laser propagation due to reflection, scattering or defocusing. Henry's law states that at a constant temperature, the amount of dissolved gas in a volume of a specified liquid is directly proportional to the partial pressure of the gas in equilibrium with the liquid. The formation of gas bubbles when water pressure decrease is also undesirable. Bubbles in the pipe and coupling head also play a negative role in waterjet ejection, laser propagation and laser-water-jet coupling. Even worse, bubbles may appear in quantity when waterjet impinge on the workpiece due to abruptly change of the water pressure. The bubbles disperse the confined laser light in the waterjet, leading a much lower machining quality. To enhance hydrodynamic and optical performance, the machine comes with a water purification system containing inverse osmoses, nano-particle filter, electro deionization, UV irradiation lamp, vacuum membrane degassing unit and active carbon filter. The produce process and qualities of the pure water is controlled by monitoring its resistivity, particle content and pH value. Water recycling is not required due to extremely low consumption.

3.2. Hydrodynamic description

A number of hydrodynamic issues are expected to confront in WJGL machining, ranging from waterjet breakup under aerodynamic forces to complex plasma formation under strong electromagnetic forces and collapse. For this section, we focus on discussing the hydrodynamic phenomena, mainly about waterjet stability. The waterjet is inherently unstable and breakup easily. To guide the laser power as long as possible, it is advantageous to suppress the breakup. Liquid jet breakup is a complex phenomenon and dependent on many intrinsic and extrinsic factors. Intrinsic factors are mainly about water hydrodynamic and thermophysical properties, such as surface tension, viscosity, density, temperature, vapor pressure, and thermal capacity, etc. Extrinsic factors involve ambient environment, nozzle geometry, and hydraulic parameters of pressure and flow rate. Physical properties of water vary with the change of temperature as shown in Table 1.

Linear stability analyses had been employed to simplify and predict a waterjet breakup for a long time due to the complex of the nonlinear phenomena and lacking of powerful computational ability. The disturbance consisting of all Fourier components is allowed to grow both spatially and temporally in the jet flows [35]. L. Ting derived and solved simplified equations governing the potential flow and the shape of slender jets of liquid, which take surface tension into account. The equations can be used to describe the flow following the breaking of jets

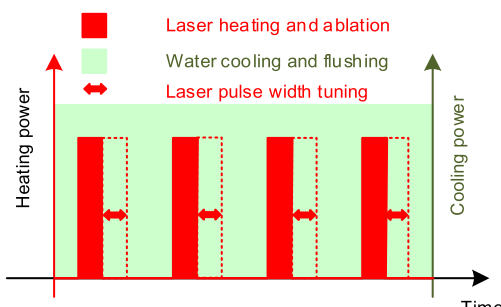


Fig. 5. Continuous alternation of heating and cooling.

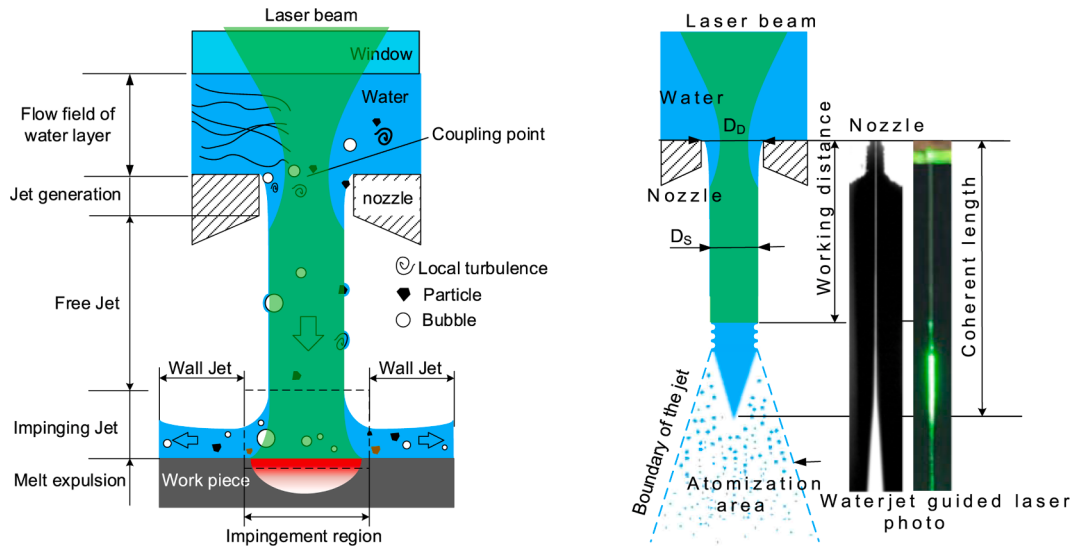


Fig. 6. Illustration of a waterjet optical fiber.

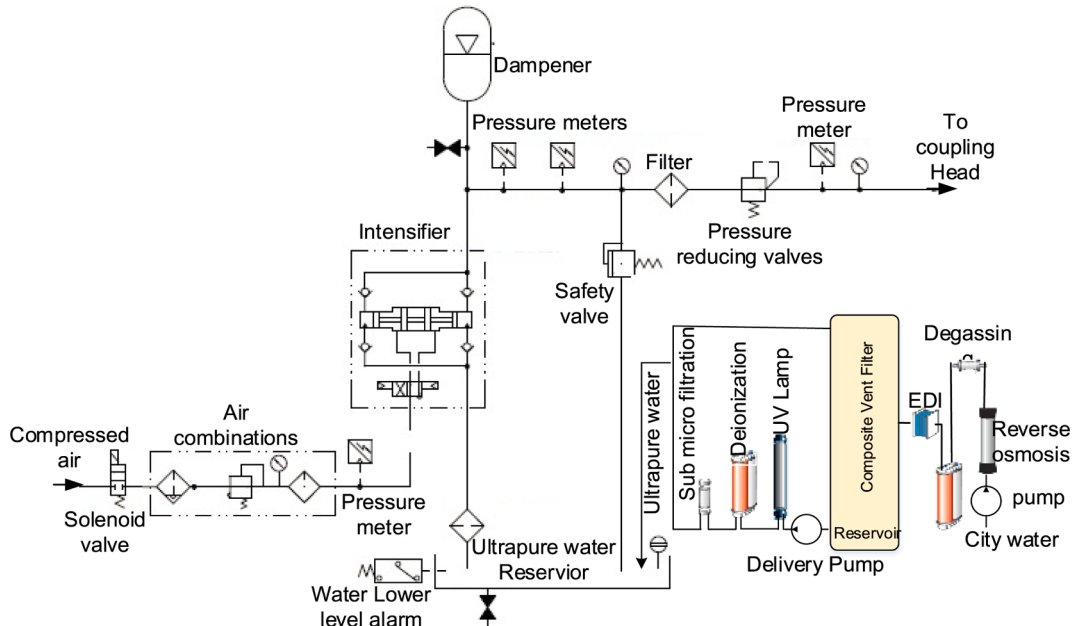


Fig. 7. The compressed water supply system.

Table 1
Physical properties of water (SI units) (Source adapted from [34]).

Temperature (°C)	Density (kg/m ³)	Dynamic Viscosity (×10 ⁻³ kg/m·s)	Surface Tension (N/m)	Vapor pressure (kN/m ²)
10	9.804	1.307	0.0742	1.23
30	9.764	0.798	0.0712	4.24
60	9.642	0.466	0.0662	19.92
90	9.466	0.315	0.0608	70.10

[36]. D.T. Papageorgiou studied analytical description of the breakup of liquid jets. Three distinct cases, i.e., inviscid jets governed by the Euler equations, highly viscous jets governed by the Stokes equations, and viscous jets governed by the Navier-Stokes equations, were constructed. Stokes jets implicitly defined closed-form solutions were constructed

which allow the scaling exponents to be fixed. Navier-Stokes pinching solutions follow rationally from the Stokes ones by bringing. The pinching solutions can be used to provide an analytical description of the dynamics beyond breakup [37]. A more comprehensive and accurate study of a waterjet is to solve the full Navier-Stokes equations expressed with eq. (3–1) and eq. (3–2) in the time-dependent fluid domain, subject to forcing at the boundary.

$$\text{ContinuityEquation : } \nabla \cdot \vec{u} = 0 \quad (3-1)$$

$$\text{MomentumEquations : } \frac{\partial \vec{u}}{\partial t} + (\vec{u} \cdot \nabla) \vec{u} = - \frac{\nabla P}{\rho} + \nu \nabla^2 \vec{u} \quad (3-2)$$

Where, \vec{u} is the velocity of the fluid parcel, ∇ indicates the gradient differential operator, P is the pressure, ρ is the fluid density, ν is the kinematic viscosity, t is the time. However, full Navier-Stokes equation can be solved theoretically only for very simple fixed domain and it is impossible for studying waterjet breakup due to the difficulty of finding

an accurate description for the fluid boundary. In addition, the waterjet column may undergo topological transitions during ejection and breakup, making the solution tougher. Thanks to the development of the computer technologies, numerical solutions become feasible although it is still significantly challenging.

Turbulence modeling is an attempt to devise a number of partial differential equations for turbulent-flow calculation, based on appropriate approximations of the exact Navier-Stokes equations. In the approach of the Reynolds-averaged Navier-Stokes equations (RANS), the flow variables are decomposed into mean and fluctuating parts followed by an averaging of the equations themselves, leading the Reynolds-stress tensor which is an unknown term that has to be modeled in order for the RANS equations to be solved [38]. M.R. Wei investigated the performance of capillary waterjets as the optical waveguide using RANS k- ϵ model combining with the fluid interface tracking method and the cavitation model. It is found when the flow velocity is large enough, the phenomenon of contraction and reattachment would lead to the formation of cavitation and the generation of the gas nucleus. The growth of cavitation region in the cavitation zone will increase the reattachment length and the distance of the hydraulic flip from the nozzle. Hydraulic flip is caused by cavitation will improve the stability of waterjet. Laminar water is successfully formed at the exit of orifice and it can be used as optical waveguide [39]. Although RANS is relatively mature, more advanced CFD modelling of waterjet breakup such as large-eddy simulation (LES) and direct numerical simulation (DNS) is still admirable to investigate the complicated morphology of water-gas interface which is critical for optical transmission, especially under hydrodynamics and high power laser thermal disturbance. F. Xiao studied liquid jet primary breakup in coaxial air flow using a developed two-phase flow CLSVOF LES methodology. A Rescaling/Recycling Method (R2M) was successfully implemented to study both liquid and gas phases in simulations of air-blast atomization. The simulated jet structures agreed qualitatively with experimental shadowgraph images and the predicted liquid jet breakup length agreed quantitatively well with experimental measurements. Instability of the water-gas interface can be investigated elaborately. It was found that water turbulent eddies existing under high Re conditions are responsible for the initial interface perturbations and, the mean shear stress from the gas flow would be the primary cause of the initial interface instability when laminar waterjet inflow occur [40]. In LES of gas-liquid two-phase jet flows, subgrid-scale (SGS) models for complex multiphase flows are still immature. There is a lack of well-established SGS models to account for the interactions between the different phases [41]. J. Shinjo investigated primary atomization of liquid injected at high speed into still air by direct numerical simulation (DNS). With sufficient grid resolution, ligament and droplet formation can be captured in a physically sound way and the physical processes can be elucidated [42]. Although DNS of multiphase flows based on the one-fluid formalism coupled with interface tracking algorithms offers a promising way forward, due to the advantageous lower costs compared with a multi-fluid approach, it also introduces severe numerical challenges and a number of obstacles should be overcome [43].

For WJGL, a fully understanding of the flow structure near and on the interfaces is very interested, rather than being averaged out in an ensemble-averaged sense. An elaborate description of the interface helps to understand how the laser power being propagated through TIR under hydrodynamic and thermodynamic fluctuation. Because of the requirements for the highly identification of interfaces, the precise numerical calculation and the detailed description are carried out in combination with an interface tracking/capturing algorithm. The most frequently employed interface tracking/capturing methods are the front tracking method by Unverdi and Tryggvason [44], the volume of fluid method by Hirt and Nichols [45] and the level set method by Osher and Sethian [46], and the coupled level set and volume-of-fluid method [47].

3.3. Waterjet into still gas

Round plain-orifice nozzles are used to generate waterjet guided the laser beam. When the water is compressed with higher pressure and accelerated through a nozzle, a free waterjet is formed as an unbroken column from the nozzle exit, and then is ruffled, and is eventually torn into small ligaments or droplets at some positions downstream. The cohesive effect of surface tension tends to pull a waterjet column into a round shape that exhibits the minimum surface energy, whilst the viscous effect of water tends to impede any change in waterjet geometry. However, external forces, such as aerodynamic forces, gravity force, and electrostatic forces, acting on the waterjet surface tend to distort and disrupt the waterjet. When a waterjet column emerging from a nozzle is exposed to a stagnant gaseous environment, the competition between the cohesive and disruptive forces will act on the waterjet surface, leading to oscillations and disturbances on the water-gas interface. The oscillations may be amplified by external conditions and disintegrates the waterjet column into droplets. This breakup process is referred to as primary breakup and has been widely investigated for over a century. Understanding waterjet breakup phenomena is very important to keep a stable waterjet column for a long extension where longer stable waterjet means longer distance the laser power can be propagated. Various simplified theories, criteria and hypotheses were proposed to explain the breakup mechanisms [Rayleigh mechanism [48], Weber theory [49], Castleman hypothesis [50], Taylor mechanisms and instability theory [51,52], as well as mechanisms proposed by Fraser et al. [53,54] by Mansour and Chigier [55], and by Faragó and Chigier [56]. Recently, more research efforts have focused on wave growth theories and thermodynamic analyses developed on the basis of experimental observations and computational fluid dynamics. When water is slowly discharged from a nozzle with a very low pressure, the gravity force exceeding the attaching surface tension force tend to tear the water into droplets, called dripping. The gravitational and surface tension forces on the drops govern the formation process of the drop and determine the drop mass and size.

Tanasawa and Toyoda identified three regimes of the jet breakup when Reynolds number is low, i.e. laminar flow regime, transition regime, and turbulent flow regime. In the laminar flow regime ($Re < 1400$), the cylindrical liquid column is transparent due to smooth water surface. The status of the laminar flow is suitable for light transmission. Bead-like swelling and contraction occur at the end of the water column, leading the formation of droplets. In the transition regime ($1400 < Re < 2400$), the laminar and turbulent flows occur alternating with random periods, rendering light transmission inefficiently. The jet breakup length decreases with increasing Reynolds number and reaches its minimum at $Re \approx 1800-2400$. Further increasing the Reynolds number, the jet flow enters into the turbulent flow regime and the jet breakup length turns to increase with roughened/ruffled jet surface and small waviness. Light transmission through the waterjet is impossible in this regime [57].

A more commonly quoted classification for jet disintegration is proposed by Ohnesorge who combined the Reynolds and Weber numbers and proposed a dimensionless number, Ohnesorge number [58]. Ohnesorge number represents the ratio of an internal viscosity force to a surface tension force physically. Depending on waterjet velocity, nozzle geometry, properties of water, and ambient environment, the disintegration of a round liquid jet in a quiescent gas are typically classified into four primary regimes, i.e. Rayleigh Jet regime, first wind-induced regime, second wind induced regime, and atomization regime. In Rayleigh breakup regime which is characterized by low Reynolds numbers, the waterjet velocities are low and only the surface tension take significant effects on the breakup of the waterjet. The breakup of the waterjet is caused by the growth of axisymmetric oscillations (varicose) of the jet surface resulting in droplets with diameters greater than the jet itself. The jet breakup length is linearly proportional to the jet velocity in this regime. In the first wind-induced breakup regime, the

aerodynamic forces on the water-gas interface becomes increasingly important due to the increasing jet velocity and the influence of surface tension is lessened. The waterjet has a sinuous wavy appearance with long breakup length. Droplets with a diameter close to the jet diameter are formed at distances far downstream of the nozzle. In the second wind-induced breakup regime at intermediate Reynolds numbers, the dynamic pressure of the surrounding air becomes predominant due to high jet velocity. The breakup of the jet is caused by the unstable growth of short wavelength surface waves due to the relative motion between the jet and the surrounding air. Droplet diameters are smaller than the jet diameter. Finally, in the atomization regime where Reynolds numbers is high, the jet breaks up in a chaotic and irregular manner within a short distance from the nozzle exit and a conical spray is formed. In practice, there is no sharp demarcation between these clearly identified regimes.

The geometry of the nozzle is the core element that allows coupling of the focused laser light into the fiber-like laminar water jet. Dual to the specificity of plain orifice nozzles, the state of the internal nozzle flow has a tremendous effect on the external waterjet flow. The plain orifice may operate in three different states as show in Fig. 8, single-phase flow when liquid fills the orifice completely, partial cavitating flow when vapor pockets form just at the Inlet Corners, and hydraulic flipped flow when downstream gas surrounds the waterjet inside the orifice [59]. The transition between regimes is abrupt, producing dramatically different waterjet formats. The internal regime determines the velocity at the orifice exit, as well as the initial droplet size and the angle of droplet dispersion [60]. The plain orifice may operate in two different regimes for guiding the laser light, i.e., single-phase with water completely filling the nozzle duct and hydraulic flipped with downstream gas surrounds the waterjet inside the nozzle duct.

3.4. Constricted waterjet

A constricted waterjet can be formed if the nozzle undergoes a hydraulic flip. Anantharamaiah simulate the waterjet inside a sharp-edge hydroentangling nozzle at pressures ranging from 10 to 200 bars ($5700 < Re < 25\,600$), the reattachment length increases by increasing Reynolds number and reaches a plateau at a Reynolds number of about 10,000. In this case the jet is first atomizing and then turns into a laminar long intact-length stream [62]. The simulation results are consistent with those of Hiroyasu's experiment as shown in Fig. 9 that even at very high liquid pressures, there exists an unbroken portion of the liquid [61].

Streamlines are unable to tightly follow sharp angles in nozzle. When fluid passes through from a sharp-edged circular orifice in a pressurized

reservoir, the gradual contraction of water takes place with the duct which is called vena contracta, resulting the decrease of the jet cross-section area. The water flow reattaches to the duct wall in the middle of the nozzle, forming a closed lower pressure vapor pocket. Cavitation clouds may occur from the tail of the cavitation film when local static pressure in the vapor pocket reach a level below the vapor pressure of the water at the actual temperature. Wavy jet is formed at the downstream since separated flow vortex shedding generates strong turbulence. For a sufficiently high liquid velocity, cavitation exists while the gas pocket continuously grows. If the duct is not long, the growing edge of the pocket reaches the nozzle exit, leading the ambient atmosphere flooding into the pocket. Hydraulic flip (super cavitation) happens and constricted water is formed. Free of the duct wall friction and cavitation, no turbulence develops in the nozzle duct and the issuing waterjet shows a smooth interface and a sudden increase of the breakup length. The breakup length of a jet is relatively long since cavitation is absent. The procedure is illustrated in Fig. 10. If the duct is long, the cavitating region does not extends down to the nozzle exit and reattach on the nozzle wall. Intense cavitation decreases the jet breakup length and increase the jet spray angle [59].

The internal state of a hydraulic flip nozzle was experimentally studied with shadow photograph. Vena contracta, cavitating cloud, and flipped flow are observed. Arai et al. noticed that the appearance of liquid cavitation at the nozzle entrance coincided with an increase of the jet angle at the nozzle exit [63]. Hiroyasu et al. (1991) called this behavior super-cavitation [64]. The procedure of hydraulic flip was simulated by Anantharamaiah [62].

Coefficient of contraction C_c is defined as the area of the stream of contracting liquid over the total cross-sectional area of the nozzle duct to represent the reduction in the cross-sectional area of the liquid jet. In ANSYS Fluent, the coefficient of contraction is expressed with Eqs. (3-3) using Nurick's fit [59,65]

$$C_c = \frac{1}{\sqrt{\frac{1}{C_{ct}} - \frac{11.4r}{d}}} \quad (3-3)$$

where, C_{ct} equals to 0.611, a theoretical constant coming from potential flow analysis of hydraulic flipped nozzles, d is the nozzle diameter, r is the radius of curvature of the inlet corner.

As a constricted jet formed, there is no wall to lead parabolic velocity profile and ideally uniform velocity distribution is attained. For a one phase waterjet, when the liquid jet emerges from the nozzle exit, the flow could be either laminar or turbulent, being governed by the Reynolds number of the flow within the nozzle. The critical Reynolds number in a nozzle duct for the laminar to turbulent transition has been

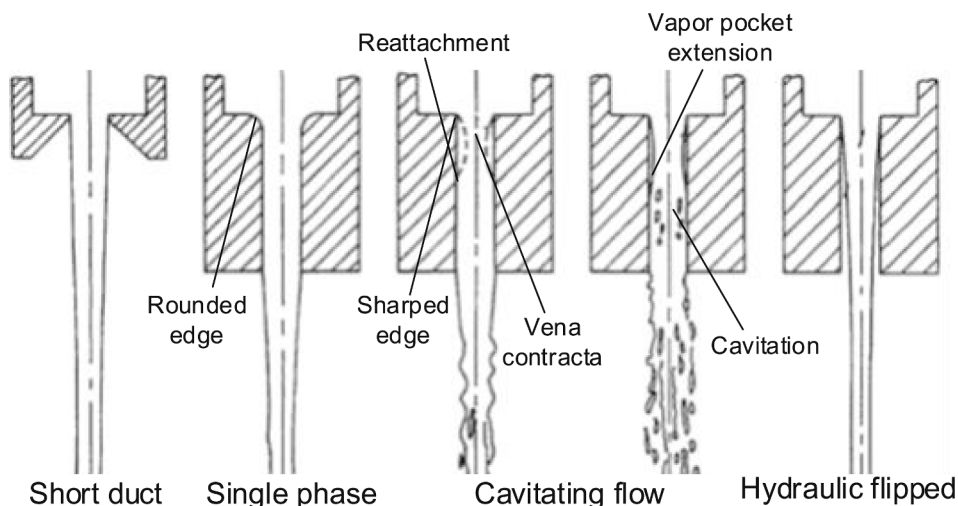
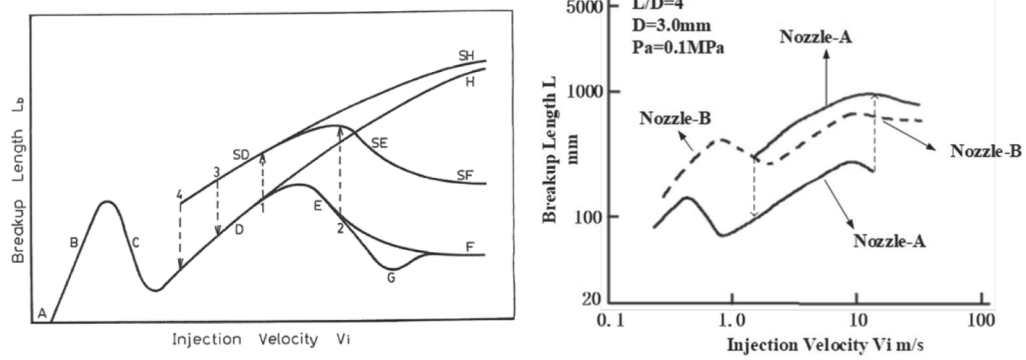


Fig. 8. Schematic appearance of the jets [61].



(a)General behavior of the breakup length (b) Breakup lengths of constricted (Nozzle A) and non-constricted (Nozzle B) jets

Fig. 9. The relationship between breakup length and injection velocity (adapt from [61]).

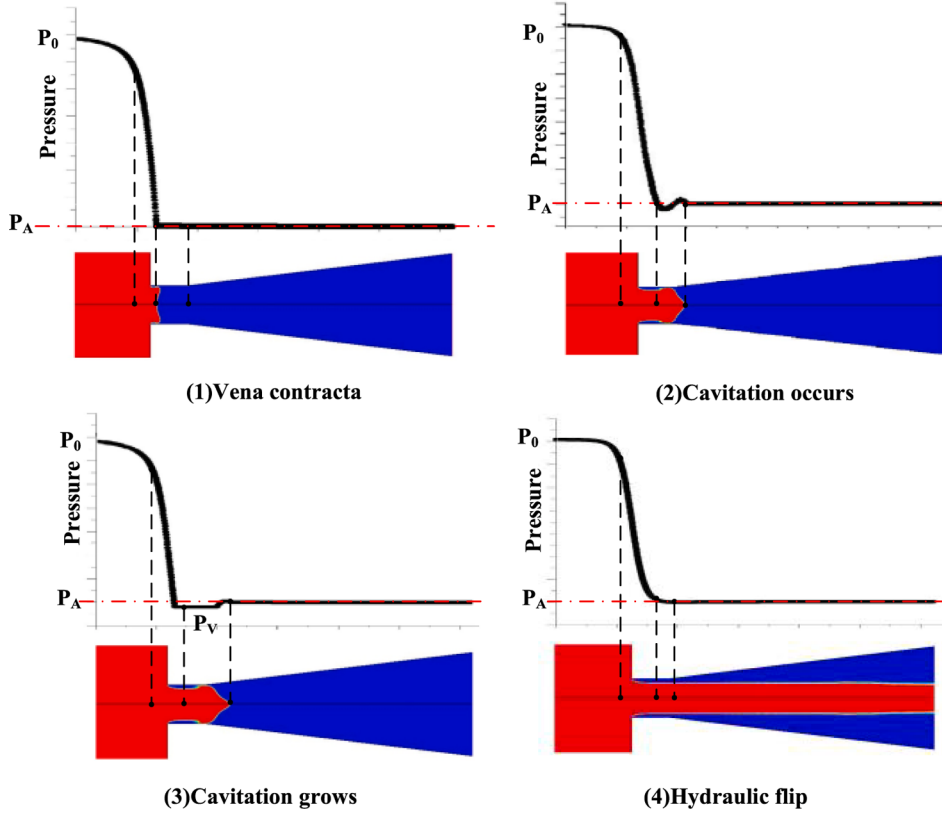


Fig. 10. The procedure of hydraulic flip.

found to be around 230. Parabolic velocity profile is formed within the nozzle due to the slip condition of the duct wall. However, the roughness of the wall disturbs the waterjet. Thus, the one phase waterjet cannot be run at high speed. The jet expulsion speed can also be roughly calculated from the water pressure P using Bernoulli's equation for dynamic pressure.

$$V \approx \sqrt{\frac{2P}{\rho}} \quad (3-4)$$

where, P is the pressure of the water, V is the velocity of the water flowing from the nozzle, ρ is the water density.

N. Anantharamaiah studied the impact forces of laminar jets in three different regions, i.e. a continuous jet, a discrete jet, and a spray region.

The impact force at continuous jet is given in Eq. (3-5) [62].

$$F_{imp} = \frac{\pi}{4} d_j^2 \rho U^2 \quad (3-5)$$

Where d_j is the jet diameter. A waterjet of 100 μm diameter moving downstream with a velocity of $U = 165 \text{ m/s}$ exerts an impact force of $F_{imp} = 0.21 \text{ N}$ on a smooth impaction plate [66].

A highly stable waterjet with a cylindrical liquid–gas interface is one of the key issues for material processing with WJGL. However, the interface is not stable with respect to external and internal perturbations, such as surface tension of the water, the velocity profile of the waterjet, the surrounding atmosphere, gravity, and electrostatic field. Due to the inherent instability of liquid jets, it is only a question of time when the interface is corrugated and torn into droplets. The distance of

the end of the continuous liquid column from the nozzle outlet prior to breakup is called the coherent length. However, not the whole coherent length can be used for total internal reflection since corrugated interface exists. Guided light is scattered out of the jet as soon as the amplitude of the surface waves exceeds a certain threshold value. The maximum distance inside the threshold value which is defined as working distance can be used for propagate laser energy with high efficiency. The temporal growth rate of the surface waves depends on the water jet's speed. An optimum in the stability curve in Fig. 11 manifests the relationship between the break-up length and the waterjet speed. Smaller nozzles exhibit their maximum at higher pressures, but the maximum obtainable break-up length is smaller than those of larger nozzle diameters. The working distance is shorter than its corresponding breakup length for a given nozzle [68,69].

3.5. Waterjet in coflow gas stream

Whether or not the gas phase is moving plays an important role in atomization since it affects the forces on the jet and, consequently, the formation, growth, and breakdown of disturbances on its surface. Traditionally, jets are broken into types based on the gas-phase environment, namely, quiescent [70,71], coflow [72], and cross flow [73].

A proper water-to-gas interface is paramount to keep the waterjet guided laser beam to the workpiece surface. Increasing the coherent length of waterjets has been subject of studies for a long time. The coaxial co-flow gas shrouding the water jet can reduce the disturbance of atmosphere and enhance the coherent length. WJGL with coherent waterjets produce fewer noise and also operate with longer working distances. Two co-flow strategies are employed in current WJGL industries. R. Cadavid showed that reducing the ambient pressure around the waterjet or surrounding the waterjet with a light gas such as Helium increases its coherent length. The coaxial gas flow decreases the relative velocity or momentum flux ratio between the gas and liquid beyond what would typically be seen in the quiescent case. Cadavid also suggested a co-flowing helium technique in which a stream of Helium is blown parallel around the waterjet using a gas collimator whose gas outlet nozzle is arranged at a distance from the waterjet nozzle [74]. Synova adopted and improved the concept as shown in Fig. 12(a) on targeting a longer, stable, and non-turbulent coherent waterjet for large working space and deep hole. [75]

However, helium doesn't have the ability to maintain water-gas boundary underwater due to its low density and relatively low kinetic energy carried to drive the water layer away. Direct-enveloping helium gas stream is insufficient to maintain water-to-gas boundary underwater. Furthermore, enveloping the waterjet with a light gas such as helium does not mitigate the problem of protecting the waterjet from motion

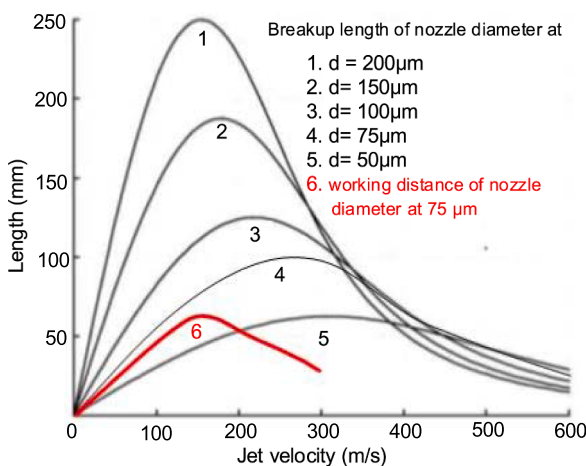


Fig. 11. Stability curves of nozzles (Revised from [67,68]).

induced friction and drag. Thus, AVONISYS has been utilizing another strategy to protect the waterjet from external perturbation as shown in Fig. 12(b). Avonisys solution is coaxial annular gas curtain of compressed air around the waterjet but without interference of with the water jet until reaching the surface of the workpiece. The waterjet and the air curtain leave the nozzles through two separate openings that are spaced apart. A noncontact, annular protective barrier is formed for the water jet inside coaxially. The atomization point defined as the position of the gas curtain intersecting with the waterjet is designed for keeping proper water-to-air interface in the working zone. Debris and backward water splashes are prevented to avoid disrupting the waterjet and damaging to the workpiece. Friction drag forces caused by the ambient environment are mitigated during relative motion of the laser head. High speed gas flow also works as driving force to evacuate the cumulated water trapped in the concave workpiece, so the waterjet can reach the surface to be processed. Even inside deep pockets, the working area of the laser is kept dry without harming the water jet's energy transmission. The air curtain seems to be a budget solution for protecting the waterjet compared to a helium shroud solution. [76]

3.6. Impinging jet

Once the waterjet impinges on the workpiece surface, the flow turns direction force. A stagnant region is formed and water enters into a wall jet region where the flow moves laterally outward parallel to the wall. The wall jet has a minimum thickness within 0.75–3 diameters from the jet axis. As the wall jet progresses, the thickness of the water film grows and its average flow speed decreases progressively according to increase of the distance from the jet center. The laser power accompanies to the pressurized waterjet column coaxially to the workpiece surface, where they reach the same area. For constricted water jet, the jet diameter contracts to about 80% of the nozzle diameter. The stagnation region is 1.2 nozzle diameters above the wall for round jets. On the workpiece, the stagnation point of the impinging water jet typically extends leads to widen 1.2 nozzle diameters of the water jet. Therefore, the kerf which can be achieved is slightly larger than the water jet itself. The generated kerf width is in average 10% larger than the water jet diameter. For example, a 30 μm nozzle generates a 25 μm water jet and a 27 μm wide cut [77].

WJGL was developed for near damage-free laser ablation due to its instinct cooling ability. The laser is used to heat and melt the material locally and the waterjet is applied to expel molten and vaporized material and, at the same time, takes charge of cooling action. Debris and contaminations are flushed away by the wall jet formed where after. Jet impingement produces high heat transfer coefficients because the impingement boundary layers are thin and the spent flow after the impingement serves to perturb the surrounding gas environment. However, the temperature field in this novel laser machining process is more complex than that of the traditional dry laser machining because of the interaction among laser, water and workpiece. The dynamic and steady temperature distribution is a crucial intermediate result that would decide the procedure and final quality of the workpiece machined. An essential quantization for understanding the underlying material removal mechanism and optimizing the process parameters is desirable. The interaction of multiphysics in WJGL involves the studies on laser power absorbed by workpiece surface, laser power absorbed by waterjet, and cooling effects by the impinging jet and wall jet [78]. These are active and promising research topics for improving the quality and broaden industrial applications of WJGL.

4. Laser-waterjet coupling and propagation

4.1. Optical characteristics of water

The refractive index varies with wavelength and temperature. From Table 2 it can be seen that the refractive index of water decreases slightly

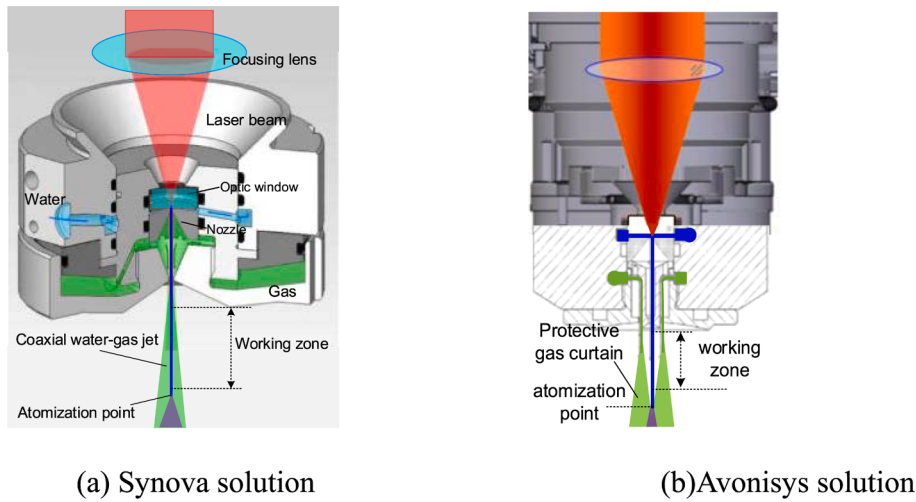


Fig. 12. Illustration of the water-jet guided laser system.

Table 2

Refractive Index of Water for Wavelength of 361 nm, 589 nm, and 1014 nm at 0.1 MPa [79,80].

Temp\Wavelength	361 nm	589 nm	1014 nm
20	1.34795	1.33336	1.32524
50	1.34373	1.32937	1.32145
80	1.33746	1.32342	1.31576

with increasing temperature.

Absorption of laser by the waterjet is an important factor when considering how much of the original laser power is transmitted to the workpiece. Fig. 13 illustrates roughly the absorption coefficient of pure water as a function of the wavelength of light. The wavelengths 532 and 355 nm are barely absorbed. However, with the high intensities of light generated by lasers, nonlinear effects can also raise the actual losses. The light transmission over a 2.5 cm water jet is as high as 99.9% at 532 nm, and 60% at 1064 nm.

The properties of the water are critical for the waterjet to transmit

the high-power laser beam, especially its thermal and optical properties as shown in Table 3.

4.2. Laser-waterjet coupling

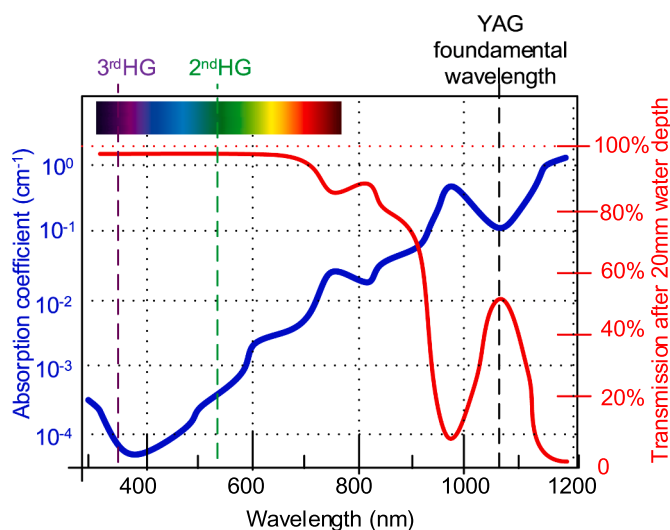
4.2.1. Coupling unit

The coupling unit mainly comprises of two major components, i.e. a pressurized water chamber and a focusing optical system. The laser beam passes through a disk-shape pressurized water chamber with an optical window on the top and a sapphire or diamond nozzle on the floor

Table 3

The properties of the water in different temperature.

Temperature T	25 °C	80 °C
Density	997.04 kg/M ³	971.79 kg/M ³
Specific Heat Capacity	4.1796 kJ/kg·K	4.1964 kJ/kg·K
Refractive Index N @1070 nm	1.3239	1.3158
Optical Penetration Depth @1070 nm	69.5 mm	93.6 mm



(a) Absorption coefficient of water at different wavelengths.

(b) Calculated transmission after 2 cm travel in water jet at different wavelengths.

Fig. 13. Absorption of laser.

and, then, is focused into a nozzle while. The geometry of the chamber and nozzle are critical to coupling the energy-rich laser beam in the water jet. A nozzle holder fixes the nozzle with orifice diameter ranging from 10 to 150 μm . The nozzle duct has an intake opening lying in an intake opening plane.

To ensure a laminar water jet being formed without induced turbulences and bubbles, the internal structure of the water chamber should be smooth and without step recesses. The nozzle duct is placed in the center of a rotationally symmetric chamber. Water is fed into the nozzle through several channels or a ring slot to suppress vortex. Although forming a laminar water jet is insensitive to the thickness of the chamber, a thin water layer is still preferable to decrease the laser absorption. Ideally, water flow forming the waterjet should bring all the laser energy to the workpiece. However, heat can be accumulated in the water chamber because of the laser absorption of materials and the coupling misalignment. If thermal flux coming into the water chamber is larger than that out of the water chamber, additional cooling strategies, such as water cooling channel in the coupling unit, should be designed. For small jet diameters and when high-power laser light is coupled into the jet with offset, laser-induced breakup can occur, leading to the premature breakup of the jet [81].

Polished sharp-edged, non-chipped sapphire or diamond nozzles are employed to form the constricted waterjet having very stable velocity profile. These features lead to a separation of the jet from the nozzle edge. In order to ensure high-quality round and laminar water jet, the nozzle holes need to be thin, non-tapering cylindrical orifice. Diamond, compared to sapphire, offers higher heat conductivity and tensile fracture strength to resist the impact of water and the thermal shock induced by the laser pulses. Since the WJGL nozzle involves medium operating pressure and high-power laser, nozzle inlets prone to some degree of wear when operating at such conditions. In order to ensure high-quality water jet, the nozzle holes need to be thin, non-tapering cylindrical nozzle orifice, round, and having a certain stiffness to resist the impact of water. The lifetime of the nozzles can last longer if the laser spot is aligned carefully with the nozzle and regularly controlled. The smallest commercialized nozzle today has a diameter of only 10 μm and further miniaturization is possible.

A transparent window provides optical path for high power laser-waterjet coupling and, meanwhile, withstands the high pressure of the water. Window thickness is determined by a combination of optical performance and mechanical strength. The laser window is exposed to substantial amounts of laser energy and high pressure of the water, thus prone to some degree of optical and mechanical damage. Thus, the optical window should be thick enough to resist distortion and break, whilst avoid to absorb much laser energy which induces significant thermal lensing issues. Fused silica is a good material for the application with its transmission ranges from 180 nm to 2 μm . Fused silica has low index of refraction, low coefficient of thermal expansion, and low inclusion content, providing stability and resistance to thermal shock over large temperature deviations. A nanostructure pattern can be created on the surface of the windows to produce a high quality antireflection effect, enabling a higher damage threshold limit than a thin film can. [82] Furthermore, fused silica can be shaped to many forms and sizes which is desirable in water chamber geometry design. Bk7 is a low cost, low performance alternative solution to fused Silica, with transmission from 350 nm to 1.5 μm . As a high-end alternative to fused Silica, sapphire can provide harder surface and longer degradation life. Unlike fused Silica, sapphire is difficult to be shaped due to its crystalline structure.

The thickness for a circular optical window can be determined with Eq. (4-1) as shown in Fig. 14.

$$T = r \cdot \sqrt{\frac{(P_{\text{water}} - P_{\text{air}}) \cdot K \cdot SF}{M}} \quad (4-1)$$

Where, T is the thickness, r is the radius of the unsupported circular area, P_{water} is the pressure of the water, P_{air} is the pressure of the ambient

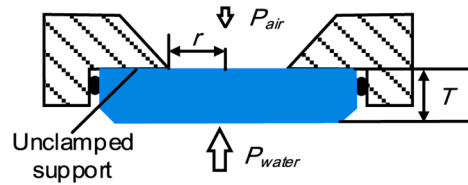


Fig. 14. Detail view of Force distribution on circular optical window.

atmosphere, $K = 1.125$ for unclamped edge, SF is the safety factor, M is the Modulus of Rupture of the window material. The O-ring seal should be able to resist the high pressure of the water in the chamber.

A typical laser optics and laser path of WJGL coupling unit is shown as Fig. 15. [83] A laser beam is first collimated in the optical head and then focused by focusing objective lenses into the nozzle opening through a transparent window. The nozzle duct inlet is illuminated with a LED and a coaxial camera to facilitate the alignment of focusing. For a collimated beam, the diffraction-limited focal spot size of a laser beam depends on its wavelength, the size of the beam at the lens and its M^2 value. When ignoring spherical aberration, the diffraction limited spot size can be calculated with eq. (4-2). For a given focal length, a larger beam diameter produces a smaller spot size, but leading the laser-waterjet coupling more difficult. For a given beam diameter, a longer focal length produces a larger spot size, but making the laser-waterjet coupling easier.

$$d_{\text{spot}} = \frac{4\lambda M^2 f}{\pi D} \quad (4-2)$$

Where d_{spot} is the diffraction-limited focal spot size, f is lens focal length, D is input beam diameter at the lens (at the $1/e^2$ point), M^2 is the beam quality factor, λ is wavelength.

Fraunhofer IPT expand the range of WJGL applications to macro laser processing by using a continuous wave infrared fiber laser source with a maximum average power about tens of kW. In a standard optical design, several pieces of optical elements are used to focusing a laser beam into a waterjet. But the solutions suffer from thermal lensing at ultra-high power due to absorption of laser radiation within multiple elements, thermal load on the laser head by scattered radiation from multiple optical surfaces and the necessity for long and complex optical

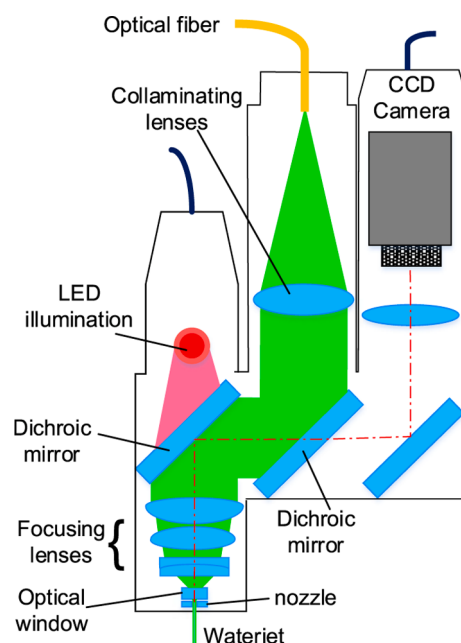


Fig. 15. A typical laser optics and laser path of WJGL coupling unit.

system with the requirement for precise alignment. Fraunhofer IPT integrated multiple optical functions into a single optical element consisting of an aspherical front surface and a tilted, spherical back surface, called “lens-prism”. A tilt of the laser beam to the optical axis by 5° has to be realized to increase the efficiency of the process. All drawbacks are addressed without a decline in image quality [84]. Y. Shen studied using non-diffracting beam generated by axicon for laser-waterjet coupling to overcome the aberration of focusing optical system and reduce coupling loss. A new design of WJGL processing system with coaxial monitoring function is proposed. Using the transforming effect on non-diffracting beam through the water fiber, the Gaussian energy distribution of laser has been altered to a flat-top energy distribution, which improves the processing quality and satisfy the processing requirements [85]. The refractive index varies with wavelength, so the laser light with different wavelength should design with different focusing objectives (lens) [86].

4.2.2. Coupling parameters

The propagation paths of laser beams in water jet can be divided into two types: the meridian ray and the oblique ray. The two different rays transmission section diagram are shown in Fig. 16.

4.2.2.1. Meridional ray.

Total reflection analysis of meridional ray transmission schematics in waterjet is shown as Fig. 17.

The coupled laser beam whose axis is parallel or with small tilt angle the axis of the waterjet. The refractive indices of water and air are approximately 1.333 and 1, respectively. The critical angle θ_c is the value of θ_1 for which θ_2 equals 90°, so Snell's law gives us the relation:

$$\theta_c = \arcsin\left(\frac{n_2}{n_1} \sin\theta_2\right) = \arcsin\left(\frac{1}{1.333} \sin 90^\circ\right) = 48.7^\circ \quad (4-3)$$

Where, n_1 is the refractive index of water, n_2 is the refractive index of air. At 48.7° and higher angle At 48.7° all light is reflected at the water-air interface and is guided along the jet.

The transparent window doesn't change the NA, but shift the focus length longer. The laser beam is refracted at the air-glass interface and glass-water interface as shown in Fig. 17.

Eq. (4-4) gives the approximate focal shift (L_e) in terms of the refractive angle (α) and the thickness (t) of the window and water layer.

$$L_e = t_w(1 - \frac{\tan\alpha_w}{\tan\alpha_a}) + t_g(1 - \frac{\tan\alpha_g}{\tan\alpha_a}) \quad (4-4)$$

Where t_w is the thickness of the water chamber, t_g is the thickness of glass.

The Numerical Aperture (NA) of a fiber is defined as the sine of the maximum acceptance angle an incident ray can have for total internal reflectance in the core. Qualitatively, NA is a measure of the light

gathering ability of a waterjet. It also indicates how easy it is to couple laser into a waterjet. From the perspective of optical fiber, the capillary laminar waterjet can be considered as a step-index optical fiber consisting of a water cylindrical core of refractive index n_{water} , surrounded by a coaxial gas cladding of refractive index n_{air} ($n_{water} > n_{air}$), Which allow more than multimode propagating through it. The characteristic of multimode fiber is that it allows propagation of light that enters within an acceptance cone of optical fiber whose value is twice the acceptance angle [87]. NA value of the water-jet waveguide and the acceptance angle:

$$NA_{waterjet} = \sqrt{n_{water}^2 - n_{air}^2} = 0.881 \quad (4-5)$$

$$\alpha_a = \arcsin(NA) = 61.8^\circ \quad (4-6)$$

Because of the refraction index difference ($n_{water} = 1.333$, $n_{air}=1$) the numerical aperture of the jet is big (0.881), which corresponds to a high acceptance angle (61.8°) for the coupling [88].

4.2.2.2. Oblique ray. Total reflection analysis of oblique ray transmission schematics in waterjet is shown as Fig. 18. The cylinder is a part of waterjet, and the arrow points to the direction in which the ray travels. Where ψ is angle between an oblique ray and waterjet, θ_w is the incident angle of ray, α is angle between HT and QT. Then, ψ can be calculated according to $\cos\psi = \sin\theta_w \cos\alpha$. On the basis of the critical condition of total reflection of oblique incident ray, α and θ_w need to satisfy the condition shown as Eq. (4-7)

$$n_{water}\sin\theta_w \leq \frac{\sqrt{n_{water}^2 - n_{air}^2}}{\cos\alpha} \quad (4-7)$$

Because the diameter of the waterjet is large compared to the wavelength of the lasers, the jet is comparable to a multimode fiber. Propagation of light in multimode fibers is usually characterized by a finite number of guided modes, refractive and tunneling leaky modes that are partially guided, and a continuum of radiation modes. For the water-jet waveguide, the number of optical modes is high. For big jets, the water jet waveguide is comparable to a large-core fiber.

There are two coupling strategies being employed for laser-waterjet coupling as shown in Fig. 19. One couples the laser beam at the entrance plane of the nozzle duct called near field coupling. The NA value of near field coupling is only decided by optical characteristics and presents a large acceptance angle. The other one couples the laser beam at the far field in the waterjet out of the nozzle duct. The NA value of far field coupling is decided by not only optical characteristics and but also geometry of the nozzle. Near field coupling enable a larger acceptant angle and a smaller focused laser beam spot size, but thermal disturbance inside the nozzle might cause waterjet breakup. Far field coupling can

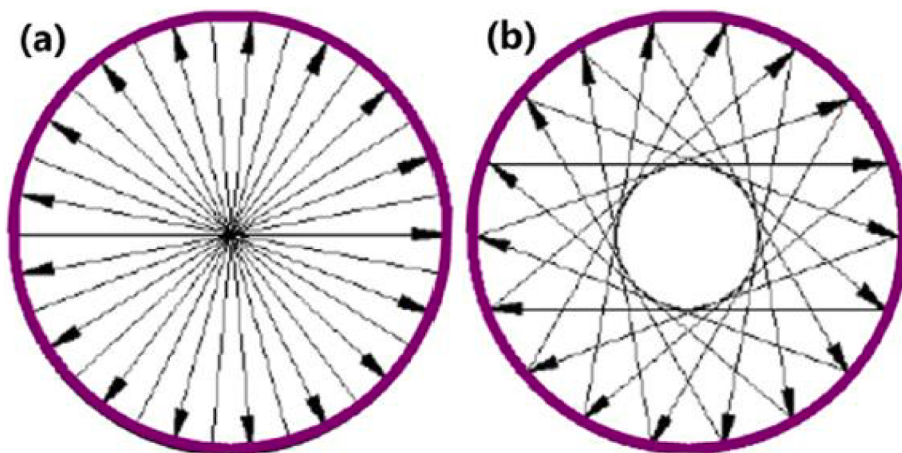


Fig. 16. Ray transmission path section (a) Meridional ray (b) Oblique ray.

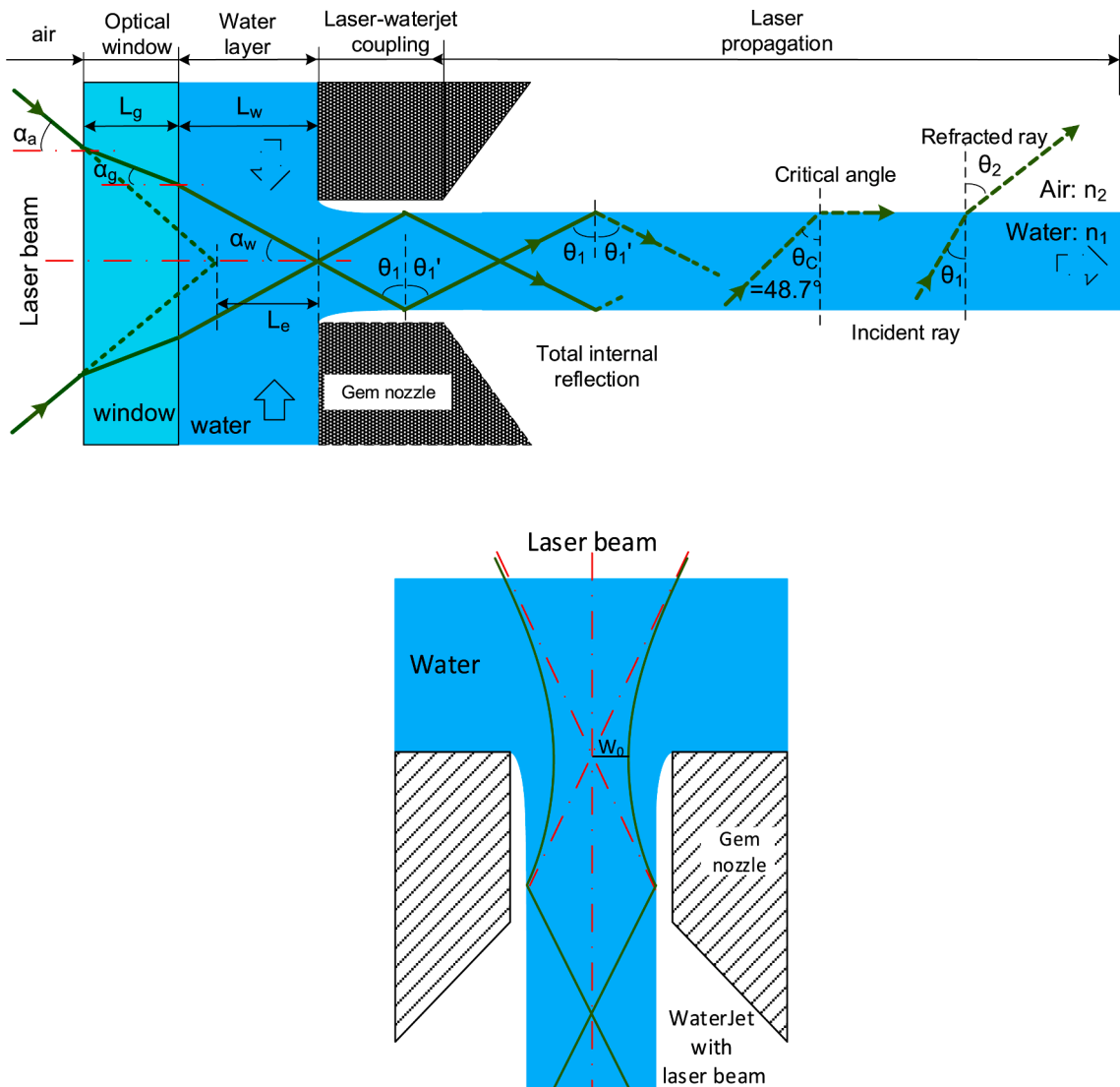


Fig. 17. Illustration of coupling the laser beam into a waterjet.

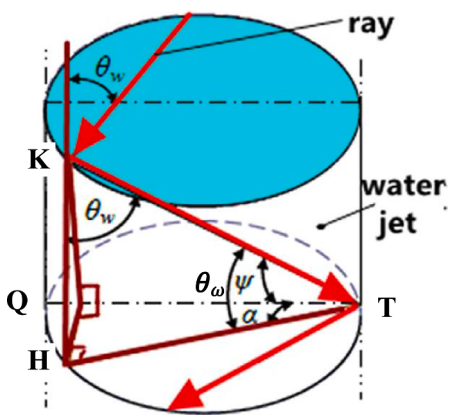


Fig. 18. Schematic diagram of oblique ray transmission (revised from [89]).

attenuate the thermal perturbation in the nozzle duct [76].

4.2.3. Coupling loss

The mechanical design of the coupling unit must ensure that the laser beam accurately and precisely aims at the end of waterjet. Laser

radiation losses occur when there are mechanical misalignments and mismatches of the laser beam and waterjet as shown in Fig. 20. The aiming errors include lateral misalignment caused by the lateral error of the optical axis of the laser beam and the central axis of the water-jet, and axial misalignment caused by the vertical spacing error of the focal spot and the water-jet end, and angular misalignment caused by the angle error of the optical axis of laser beam and the central axis of the water-jet. The coupling mismatches include NA mismatch when the transmitting laser beam has an NA greater than the NA of the waterjet, and laser spot size mismatch when focused laser beam waist is larger than the size of the waterjet. Coupling misalignments and mismatches might lead the high power laser leaking from waterjet or touching the edge of the nozzle directly, causing the turbulence and the damage of the nozzle, ever worse, destroying the optical window due to splash debris in the water chamber. For single phase waterjet, laser will touch the nozzle wall if the coupling point is settled in the nozzle duct by mistake [90,91].

An experimental setup was designed and implemented by N. Vágó, etc. for performing breakup length measurements of free liquid jets with the light-guided method and with shadowgraph imaging simultaneously. The light leaving the jet perpendicular to its axis indicates the breakup point. A ray-tracing program demonstrated the principle of the experiment and predicted the applicability for non-axisymmetric modes

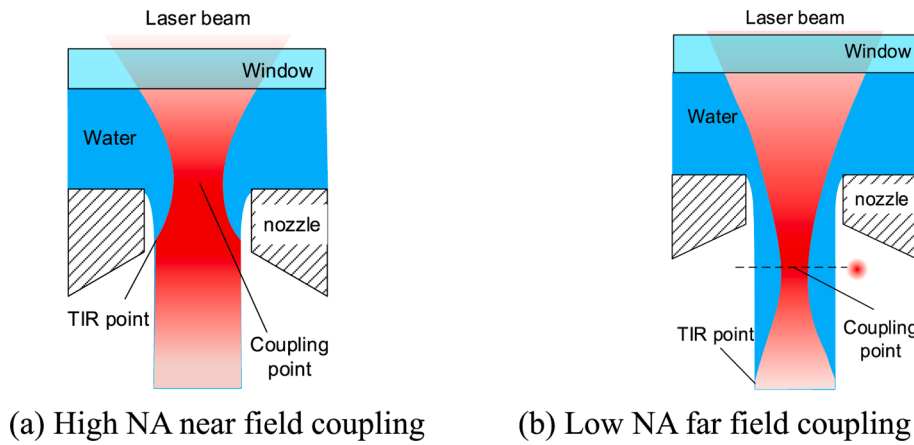


Fig. 19. Laser-waterjet coupling strategies.

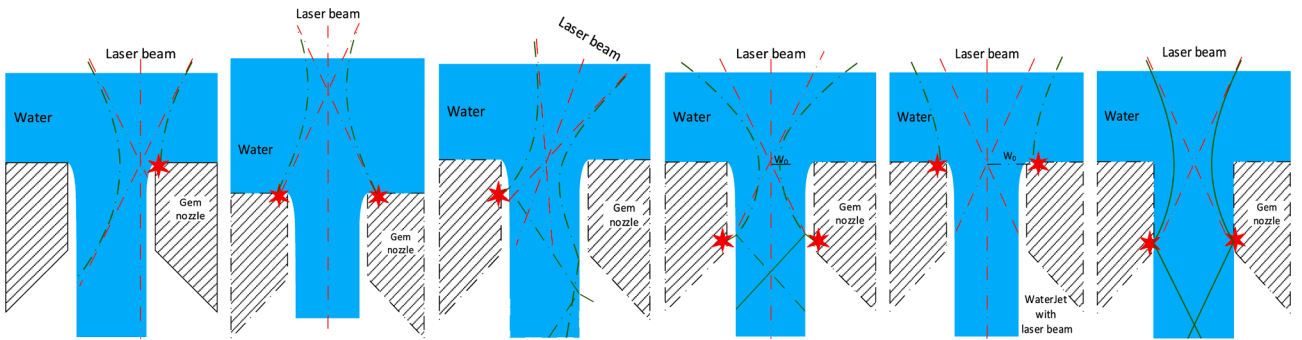


Fig. 20. Principle view of lateral error, vertical spacing error and angle error.

in the first wind-induced breakup regime [88]. P. Couty, etc. conducted experiments on investigating laser-induced break-up of water jet waveguide using the setup. Laser pulses lead to different break-up characteristics when the coupling configuration with respect to the jet axis was changed for the same average power, peak power, and repetition rate of the laser. It is found the controlled jet is not only sensitive to the laser peak power but also to the precision of the laser-waterjet coupling. The energy transfer from the laser pulse to the water during the coupling can be explained by both the absorption of water with the high intensity pulses and the localized heating of the nozzle edge [92]. For being able to transport high power laser radiation through a waterjet, an enough volume flow rate has to be guaranteed in order to prevent heat accumulation in the water chamber, keeping water temperature below the boiling point and avoiding vapor bubble formation. Higher temperature may cause unstable flow and weaken the focusing condition. When the focused laser spot is well centered and funnel into the waterjet, little laser energy distribution will overlap the nozzle edge. However, when off-center coupling is set, a significant amount of the total energy may be absorbed by the surface of the nozzle, leading to local thermal stress and deformation in the sensitive region where the jet is produced. Even transparent material such as optical window and nozzle can be damaged by high power laser absorption. Moreover, the possible hot sources can result in a non-symmetric hydrodynamic disturbance that cannot be ignored for the jet stability. At the position where the high power laser passes, the temperature change in water induces a negative refractive index change called thermal lensing, resulting in an expansion of the laser beam strong enough to render the coupling completely inefficient [93]. Turbulence is a kind of instability flow with changeable refractive index. Turbulence in the water chamber may be formed by thermal effects, unsmooth surface, damaged nozzle, or laser-induced bubble, as shown in Fig. 21. When laser beam transmit through the turbulence or bubble area, the direction, phase and intensity

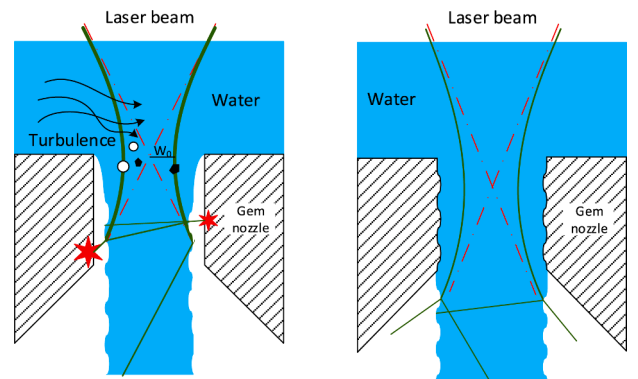


Fig. 21. Principle view of lateral error, vertical spacing error and angle error.

profiles are changed, causing defocusing of the laser beam [17,93–97].

4.3. Laser propagation in waterjet

4.3.1. Propagation modes and speckle

A meridional ray is a ray that passes through the axis of an optical fiber. A skew ray is a ray that travels in a helical path and never crosses the axis of an optical fiber, greatly outnumbering meridional rays. The diameter of the jet is large compared to the wavelength of the lasers, the jet is considered as a multimode fiber. Propagation of light in multimode fibers is usually characterized by a finite number of guided modes, refractive and tunneling leaky modes that are partially guided, and a continuum of radiation modes.

A normalized frequency parameter, which determines the number of modes of a step-index fiber. The V of a step-index fiber is a normalized

frequency parameter which describes the number of guided modes.

$$V = \frac{2\pi}{\lambda} aNA = \frac{2\pi}{\lambda} a \sqrt{n_{water}^2 - n_{gas}^2} \quad (4-8)$$

Where λ is the laser wavelength, a is the radius of the waterjet, and NA is the numerical aperture. For $V < 2.405$, a fiber supports only one mode per polarization direction. Multimode fibers can have much higher V numbers. Multimode step index fibers have values $V > 2.405$ and can sustain many modes simultaneously.

$$V_{UVlaser} = \frac{2\pi}{\lambda} aNA = \frac{2\pi}{0.355} 5 \sqrt{n_{water}^2 - n_{gas}^2} = 77.57 \quad (4-9)$$

$$V_{greenlaser} = \frac{2\pi}{\lambda} aNA = \frac{2\pi}{0.532} 5 \sqrt{n_{water}^2 - n_{gas}^2} = 51.76 \quad (4-10)$$

$$V_{infrared} = \frac{2\pi}{\lambda} aNA = \frac{2\pi}{1.064} 5 \sqrt{n_{water}^2 - n_{gas}^2} = 25.88 \quad (4-11)$$

Waterjet multimode fiber have large difference of refractive index between water and air and large numerical apertures, making them well suited for collecting light from large or diffuse sources. They are also well suited for high power applications as the power is transmitted through a large cross section compared to single mode or polarization maintaining fibers [98]. The coupling unit is very similar to a usual fiber-coupling unit, except that the intensity distribution of the light in the nozzle is flat-top and not Gaussian, due to the mode mixing in the fiber delivery of the laser and the imaging properties of the setup [99].

4.3.1.1. Size of speckle grains and affecting the ablation results. The advantage with multimode fibers is that they do not maintain the spatial properties of Gaussian lasers. Instead the light is dispersed among multimode modes within the fiber, generating an out-speckle pattern when the light emerges from the other end of the fiber. Lasing mode distribution: It influences the ablation critical dimension and the precision in the ablation depth determining substantially the intensity distribution along the laser spot on the surface and its uniformity, the presence of the speckle phenomenon can be a problem in case of multimode lasers; generally a high-quality process is easier to obtain using a single mode laser. [100]

Compared to Gaussian beams, flat top beams have a constant irradiance profile through the cross-section of the laser beam, resulting in more accurate and predictable results. Some applications benefit from a constant intensity over a given area, such as the processing of semiconductor wafers where cleaner cuts and sharper edges are required. The light distribution profile emerging from the waterjet waveguide depends strongly on the coupling parameters of the focused laser beam. The condition to obtain a constant irradiance intensity profile at the output of the waterjet is to excite a maximum number of modes. The numerical aperture (NA) of the coupling of the laser source into the water jet waveguide is the predominant parameter influencing the grain size of modal noise in intensity distributions. It was proved experimentally and theoretically by P. Couty that higher the NA produces smaller speckle sprays. As the diameter of the water jet is increased, more modes are accommodated, resulting in modal noise where corresponding speckle grains of small size are present. Better homogeneity of the modes over the entire water-jet section is obtainable by decentering the coupling, although overlap of the focused spot with the nozzle edge should be certainly be avoided. The size of the speckle grains along the waterjet remains constant. Shifting the focus along the jet axis has no effect on the grain size [81].

4.3.2. Propagation attenuation

Laser power attenuation or loss caused by absorption and scattering happens when laser light propagation travels along a waterjet column. The main cause of intrinsic absorption is the characteristic vibration frequency of water. Extrinsic absorption is caused by impurities

introduced into the waterjet. Scattering losses are mainly caused by the interaction of light with impurities, turbulence, and bubbles. In addition, for the ultrahigh power laser radiation via a water jet with a long transmission path, stimulated Raman scattering is observed. The deformation of a waterjet column, such as corrugated water-gas interface, bend waterjet column with small radius of curvature, also causes attenuation.

4.3.2.1. Absorption. The Beer-Lambert law relates the attenuation of light to the properties of the material through which the light is travelling. Although the absorption coefficient for the laser wavelength 532 nm in water is about 0.0004 1/cm, there is a threshold for the light to be non-linearly absorbed when high intensity light is involved [101]. Using Beer-Lambert's equation, it is possible to calculate how much of the original laser power actually reaches the workpiece, such that:

$$P = P_0 e^{-ad} \quad (4-12)$$

Where P is remaining power, P_0 is original laser power, e is Euler's number(2.718), a is absorption coefficient, d is distance penetrated in water. The main absorbance equation is the Beer Lambert Law which is:

$$A = \epsilon lc \quad (4-13)$$

Where A is the absorbance, ϵ is the molar absorptivity constant. This is different for every chemical, and at every wavelength, l is the path length, the distance of solution that the light has to travel through, c is the concentration of the solution.

Thermal model of a high power laser beam guided in a water jet. For being able to transport high power laser radiation through a Laser Micro Jet (LWJ), a high enough volume flow rate has to be guaranteed in order to keep water temperature below the boiling point and avoid vapor bubble formation. Due to the primary important of flow rate, the nozzle diameter should be designed to ensure the required flow rate and pressure should be chosen to maximize the breakup length. As the laser power loss is basically independent of the jet parameters (except temperature dependent absorption), transmission length has to be kept low in order to maintain good optical transmission efficiency. The power loss can be reduced by allowing a certain temperature increase until the working position of the LWJ, minimizing temperature dependent absorption.

For the transmission of 30 kW laser radiation via a water jet and a transmission length of 50 mm, a minimum nozzle diameter of 1 mm has to be used at a pressure of 50 bar. The jet reaches a temperature of 88 °C and the laser beam experiences a power loss of approximately 45%. When using a bigger nozzle diameter of 3 mm and a pressure of 100 bar at the same transmission length, temperature rises to only 31 °C but the power loss increase to 50% [96].

4.3.2.2. Thermal induced waterjet perturbation and breakup. A water jet tends to be disturbed when a high laser intensity is coupled in it, especially for IR laser with a high absorption coefficient, due to thermal fluctuation. Once a perturbation is triggered, it travels along the surface of the water jet to the downstream and is amplified exponentially by the interaction of surface tension and ambient pressure. When the surface deformation of the waterjet column is large enough, leading total internal reflection impossible, laser light starts to scatter out from the waterjet and less laser power is transmitted to the workpiece. Maximal working distance of the waterjet and cutting quality are significantly reduced. [102]

M. Maier and W. Kaiser found the threshold of simulated Raman scattering in pure and mixed liquid is proportional to the reciprocal Kerr constant [103]. J.S. Bartlett et al. found the absolute magnitude for Raman scattering coefficients of pure water to be $(2.7 \pm 0.2) \times 10^{-4} \text{ m}^{-1}$ for an incident wavelength of 488 nm [104]. V.A. Babenko et al. conducted experiments on non-stationary stimulated Raman scattering (SRS) of laser pulses to investigate whether the water sample with

bubston phase and found the SRS excitation threshold in water with the bubston phase turns out to be higher than that without buston phase [105]. Å. Spiegel studied red light with wavelength around 653 nm emitting from the stable portion of the jet when a 532-nm green light of a frequency doubled Nd:YAG laser was coupled into a thin water jet. The intensity of the red light induced by nonlinear optical effects grows as higher input green laser peak intensities of 1.3 GW/cm^2 are approached. The power loss in the form of stimulated Raman scattering at high intense pulsed laser beam is significant and enhanced by the long interaction length in the water jet, influencing the cutting performance of a WJGL cutting. At high power, approximately 30% of the input light irradiance is lost, turned to secondary red light and dissipation [102]. U. Eppelt constructed a model formulation for the diffraction of the radiation within the propagation along the resulting water jet. However, the academic results are not disclosed. [106]

5. Laser-matter interaction

5.1. Laser source

Although WJGL ablation principle seems quite simple, the laser sources are chosen carefully for the application and the cutting requirements, depending on the compatibility to lower absorption of the water for this wavelength and the workpiece material behavior. The employment of water as the jet medium enables a large range of laser types to be used because of its wide transmission window. The WJGL have been put into operation with conventional lamp pumped or diode pumped lasers with pulse durations in the micro- or nano-second range, operating at 1064 nm (fundamental frequency, near infrared), 532 nm (frequency doubled, green), or 355 nm (frequency tripled, ultraviolet) [107].

Disc and fiber lasers (emitting at 1,070 nm) and continuous wave (CW) YAG Laser also have been deployed with success in specific applications. In addition to the absorption coefficient, the optical penetration depth varies with wavelength, and different ablation results are expected for ultraviolet, green and infrared lasers. The most commonly used commercially available lasers for WJGL cutting is the diode pumped solid state pulsed green Nd:YAG lasers with average laser power ranges from 10 W to 500 W because of their good pulsing properties and excellent compatible with the water transmission spectrum.

UV lasers are superior to green or IR lasers for cutting materials that have a low absorption coefficient or are transparent at 1064 and 532 nm wavelengths, such as copper, polyimide, sapphire or glass [108]. However, UV lasers are still slow and do not provide enough output power for an efficient material processing. Near-Infrared lasers around 1064 nm are fast and powerful. However, only a fraction of the power is delivered to the workpiece due to relatively higher water absorption. High absorption of high power IR laser creates water vapor bubbles which may create unstable water flow and nozzle damage. CW laser ablation suffers of the fact that the substrate heating is maximized, thus only suitable for materials with good thermally conductivity [96]. Advantages of fiber lasers is flexibility, easy beam delivery, compact size, reliability and vibrational stability. [109] Pulse lasers with pulse widths gained more attention for WJGL compared to continuous wave because a better finish is attained as the jet cools the material during pulsating period. High power long pulse radiation can be achieved relatively high production rates but with low quality. Shorter pulse length lasers are used for applications requiring high precision and high kerf quality. Shorter wavelength laser is also catered for focusing, fiber transmission and metal surface absorption, enabling higher efficiency. The WJGL system is based on more powerful and more economical industrial lasers, rather than expensive ultrafast pulse laser sources, enabling a significant higher speed.

5.2. WJGL ablation and simulation

5.2.1. Common WJGL-matter interaction

Laser cutting uses a focused high-power-density laser beam to illuminate a workpiece, causing the material to be irradiated to rapidly melt, vaporize, ablate, or reach a flash point. At the same time, the molten material is blown off by a high-speed airflow coaxial with the beam, thereby cutting the workpiece. Laser cutting is one of the hot cutting methods. The procedures are divided into three: [110]

- (1) **Laser vaporization cutting:** High intensity focused laser beam evaporates the material and blow it out by expansion and/or the gas jet.
- (2) **Laser melting cutting:** Laser beam provides necessary process energy. An inert cutting gas jet forces the melt out of the kerf.
- (3) **Laser beam oxygen cutting:** The material is heated to the ignition temperature to initiate an exothermic reaction with the reactive cutting gas. This reaction influences the viscosity of the melt and the absorption conditions, and additional process energy is provided. The gas jet removes the reaction products from the cut kerf.

Due to the unique properties of the laser beams (such as coherence, monochromaticity and collimation) they are applied in several research and practical fields. The use of laser cutting to process brittle materials (such as ceramics, semiconductors and glass) has better advantages in mechanical machining. However, laser cutting of brittle materials is often accompanied by undesirable consequences, such as micro-cracks, deviation of the cutting path and thermal effects, splashes and debris. To alleviate the above problems, various technologies have been adopted, such as thermal evaporation / melt injection and controlled fracture. The experimental results show that a single crack is generated at a temperature far below the melting or phase transition temperature, and volume absorption can quickly cut transparent and translucent materials. [111] In this way, high-quality "stealth" cutting can be achieved without debris. At the same time, due to laser cutting of brittle and low thermal conductivity materials, high thermal gradients will generate thermal stress, but this stress can be avoided with the help of water.

Carbon or glass composites are increasingly used in the aerospace, energy, automotive and sports industries due to their light weight and acceptable strength. In laser cutting of carbon fiber and glass fiber composite materials, due to the large difference in material properties between carbon fiber or glass fiber and its polymer binder, cutting becomes complicated. The excessive heat conducted by the fiber during laser cutting will negatively affect the polymer binder, which causes the fiber to form a larger heat-affected zone. Although short pulse high-speed cutting can minimize thermal effects, the material removal rate is not yet commercially competitive. Compared with mechanical and waterjet cutting technologies, WJGL technology has better quality and faster speed.

Process requirements in the aerospace industry, the automotive industry, and the electronics industry have led to the development of laser drilling technology. Compared with other drilling techniques, laser drilling has the characteristics of fast speed and little damage. However, laser drilling also carries inherent problems with laser processing (e.g., recasting, debris, hole cones, heat affected zones). Therefore, the addition of coaxial water jets in the laser drilling can help wash away impurities, eliminate thermal effects and form parallel holes [112].

In the laser cutting process, metals such as aluminum and alloys are the most used materials in the industry, but the high reflectivity and electrical conductivity of these materials affect the cutting process. In traditional laser cutting, certain metals will become vapor or melt during the cutting process. When thicker materials are processed and a large amount of materials are melted, the laser functions like a plasma cutter.

According to the manufacturer, the laser pulse forms a plasma when it comes into contact with the workpiece, which instantly separates the

high-pressure water jet from the workpiece. After each pulse, the waterjet cools the surface and discharges the cutting waste with a smaller but more concentrated force than the cutting gas [113].

5.2.2. Modeling of material removal

Optical absorption properties of metals. In general, metals absorb laser beams with short wavelengths. Therefore, selecting a wavelength suited to the absorption properties of the material to cut makes actual cutting easier. If the thermal conductivity is high in a material such as aluminum, much of the energy is transferred laterally into the material, which results in inefficient cutting and reduced cutting speeds. As a general rule, if energy is transferred into a material inefficiently, the effectiveness of the cutting process is reduced.

Two volume parameters as material removed per pulse estimated with energy (MRP_e) and material removed per pulse estimated thermally (MRP_{th}) as shown in Eqs. (5-2) and (5-3). The definitions using volumes provide an intuitive link to process performance. In the literature, they are often used in the form of Fluence and Fluence Threshold [114].

$$\delta_{th} = 2^* \sqrt{D^* t_p} \quad (5-1)$$

$$MRP_e = \frac{T^*(1-R)^* P_L}{\rho^*(c_p^* T_v + L_m + L_v)} \quad (5-2)$$

$$MRP_{th} = \pi^*(0.4^* d_n + \delta_{th})^2 * \delta_{th} \quad (5-3)$$

$$MRP_{fit} = DistributionPulses * PressureParameter * MRP_e * e^{-0.1^* \frac{MRP_e}{MRP_{th}}} \quad (5-4)$$

Where P_L is laser average power, f is laser pulse rep. rate, t_p is laser pulse duration, d_n is jet nozzle diameter. And the density ρ ; thermal diffusivity D ; the boiling temperature T_v ; the heat of fusion L_m and vaporization L_v ; the specific heat C_p ; as well as reflectance R and optics transmission T as [0–1] values.

Fig. 22 graphically defines the other two parameters. They are dimensionless pulse distributions and dimensionless pressure parameters. These parameters include water pressure, plasma pressure, machining speed, tool step, jet width and so on.

The resulting model described by Eq. (5-4) estimates the Material Removed per Pulse (MRP_{fit}). The rate of material removal is controlled by the laser processing parameters, such as laser power and processing and scanning speed, and is not affected by the maximum tool force, tool chatter, and built-up edge formation [112].

Jeremie Diboine et al. [114] proposed a model that is fitted using a database of milling and drilling experiments on aerospace nickel alloys and thermal barrier coating (TBC) ceramic materials. The model is built around the well-known energy balance approximation [115], as well as the 1D thermal diffusion parameters. And the model has successfully used predicted aspects of free-shape machining such as depth and controlled angle and has evidenced the wall effect and its main causes during 2.5D shape machining with the Laser MicroJet®.

Implementation of Taguchi methodology performed by Dubey and

Yadava [116] in cutting aluminum alloys with Nd: YAG laser, thus finding the optimal processing conditions to optimize the quality characteristics. They showed that material removal rate is primarily determined by the cutting speed but the kerf taper is only determined by the pulse frequency. Other authors such as Hsu and Molian [117] and Ilavarasan and Molian [118] explored the performance of noncoaxial nozzles in conjunction with conical coaxial nozzles to improve material removal and cut quality.

A stable laser cutting process is described theoretically by the power balance of the incoming and outgoing power contributions, i.e., the laser beam energy absorbed in the material has to be equal to the energy necessary for heating and transforming the material along the cutting process. The most general expression of the power required for a conventional laser cutting is:

$$AP_L + P_r = P_{Tm} + P_m + P_v + P_l \quad (5-5)$$

The terms in the left side are the absorbed laser power AP_L and the power P_r of the exothermal reaction in the case of oxidation cutting, while the terms in the right side account for: (1) heating the material from room to the melting temperature P_{Tm} , (2) the latent heat of melting P_m , (3) heating the melt to the vaporization point P_v , and (4) the latent heat of evaporation P_l . This equation gives a rough approximation of the energy required for the different processes of material transformation, and does not take into account losses, the duration of irradiation, and the energy distribution in the laser beam. A more detailed and accurate analysis, based on the energy conservation, should include also these factors.

The theoretical description of the water-jet guided laser cutting given below is based on the assumption that the cutting occurs at evaporation and the water jet removes the ablated material. Also, bearing in mind that the laser beam is confined into a water-jet undergoing multiple reflections like in an optical fiber, we assume that the distribution of the laser energy across the water-jet is constant. Another factor, simplifying the analysis, is the alternation heating and cooling effect due to the pulse working regime used in the MicroJet® cutting. During the pulse duration the laser beam is absorbed and interacts with matter as in the case of conventional laser cutting. Between the pulses, though, the waterjet instantly cleans and cools the kerf, and therefore, the accumulation of heat accumulation might be ignored and any following cycle might be considered independently from the previous one. The equation of the power balance that describes the water-jet guided laser cutting could be obtained from Eq. (5-6) bearing in mind the assumptions above:

$$tAP_L = \rho V [C_p(T_m - T_0) + L_m + C_p(T_v - T_m) + L_v] \quad (5-6)$$

where A is the material absorptivity of the laser energy, PL is the laser beam power, ρ is the mass density, V is the volume of the removed material, C_p is the heat capacity, T_m and T_v are the temperature of melting and evaporation, respectively, T_0 is the room temperature, L_m is the latent heat of fusion and L_v is the latent heat of evaporation. The total interaction time t , also taken into account, represents the time required for the cutting front to move to a distance l with speed v , thus, $t = l/v$.

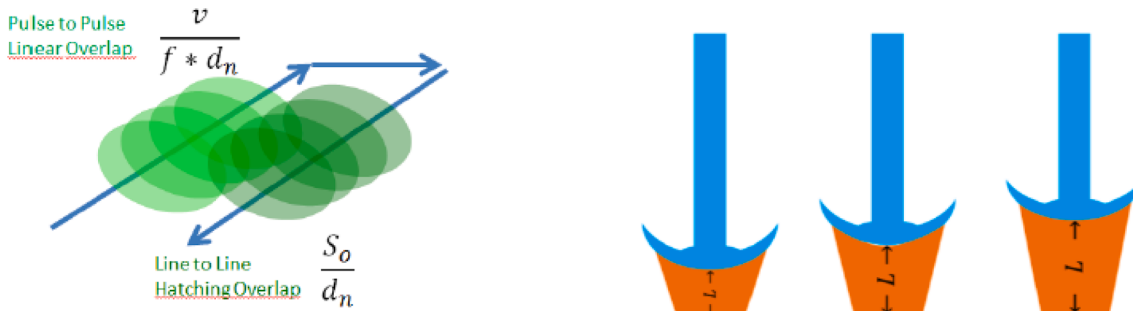


Fig. 22. (left) dimensionless Distribution of Pulses; (right) dimensionless Pressure parameter (resource from [114]).

The mass of the removed material is $V = whl$, where h the material thickness, and w is the kerf width. At best working conditions, the kerf width is the same as the diameter of the water jet, which is equal to the nozzle diameter D , i.e., $w = D$.

The development of a process for a specific application is complicated by the multitude of process parameters involved. Historically, satisfactory process parameters for a specific application have been based on empirical knowledge and experience. Due to the increasing use of lasers in commercial production and in the continuing development of new applications, there is significant interest in the development of models that can describe the complex laser–material interactions well enough to guide the selection of process parameters. Since laser material processing is a transient process that involves transmission, absorption, and reflection of radiant energy; conduction, convection, and radiation of thermal energy; temperature-dependent material properties; moving boundaries; melting; fluid flow; vaporization; and gas dynamics.

C.F. Li et al. simulated the heat transfer of waterjet guided laser processing silicon, determined its cooling effect, and compared the simulation results with the experimental results [119]. H. Zhu et al. carried out a numerical simulation study of the heat transfer and material ablation in a hybrid laser-waterjet microgrooving, the results shown that heat accumulation in the workpiece is effectively removed by the waterjet cooling effect during the off-pulse period, and therefore the thermal damage caused by laser heating was minimized [120].

C.F. Li [21] and Y.K. Madhukar [122] investigated a study for waterjet assisted laser grooving of silicon that treats the energy input of the laser, the cooling effect of the waterjet, and the melting and removal of the silicon and excellent agreement exists between the simulated and experimental values of the width of the groove at the surface of the workpiece.

J.A. Porter, performed an experiment of cutting thin sheet metal with a water jet guided laser using various cutting distances, feed speeds and angles of incidence. Although the higher feed speeds reveal even a short disturbance as a discontinuity in the kerf, the feed seems to have much less significance than the cutting distance in the tested feed range. Admittedly, all the cutting speeds used provided multiple overlapping of the laser pulses as presented in the experimental procedures section. The material in question is 0.1 mm stainless steel and the cutting distance is 30 mm. The feed is so fast that individual pulses can be identified in the kerf. Despite the high feed, individual pulses manage to penetrate the material. However, insufficient pulse overlap causes a splash of melt to solidify on the upper side of the material, probably before the material is penetrated. Pulse overlap is thus required to enable the water jet to pass smoothly through the material, expelling the melt with it [113].

5.2.3. WJGL parameters for cases

The mild processes and high-quality performance results allow WJGL to process a broad range of materials, including semiconductors, natural

diamonds, synthetic ultra-hard materials, advanced composites, metals, and ceramics.

The industrial application of WJGL processing is established already. However, there are gaps in understanding the physical mechanisms involved in laser ablation, especially issues related to the realization of desired ablation contours and maximum ablation depth. Modeling and simulation can offer an appropriate gain in process understanding. The models elaborated for the demonstrated application cases give an insight how crater shape, morphology of the ablation front and damage within the material evolve.

Ablation ability and quality, kerf size and geometry are determined by material properties of the workpiece and appropriate selection of the cutting parameters, such as laser type, average power, peak power, pulse width, repetition frequency, pulse duration, nozzle size, and water pressure, etc. Laser power utilization and fluidal (water or gas) pressure are often optimized for the cost of operation and or efficiency. In Table 4, the parameters for a few cases are listed.

5.2.4. Laser induced bubble and breakdown

Though water can cool the workpiece during the ablation, the thermal and hydrodynamic features of water can adversely interfere the laser beam transmission. The bubble formation is hardly prevented since it is a consequence of the vaporization of water and workpiece material under the intense laser radiation. High power laser energy increases the temperature of the water, making the cavitation trend to happen. Although the vapor bubbles collapse also help to expel the molten materials, the bubbles created in water can scatter the laser power and in turn attenuate the laser intensity at the work surface and subsequently lower the ablation quality. Understanding the laser–material–water interactions and the behavior of bubbles during the laser ablation in water could essentially be useful for further improvement of WJGL technique. As a solution, the water with a degassing system is highly recommended. For being able to transport high power laser radiation through a WJGL, a high enough volume flow rate has to be guaranteed in order to keep water temperatures below the boiling point and avoid vapor bubble formation [113,120,130].

When approaching high power laser irradiation, electron density in the water reaches a critical value resulting in cascade ionization and water breakdown. Bubbles can be nucleated and created by forcing the dielectric breakdown of water into plasma. This breakdown plasma in the water shields laser propagation and results in an attenuation of the transmission. The bubbles behaved like cavitation bubbles, growing, collapsing, and then generating a shock wave. However, the effect of laser induced water breakdown can be ignored at present because water breakdowns on 1064 nm, 532-nm wavelength and 355 nm occur at approximately 10 GW/cm², 6 GW/cm², 4 GW/cm², respectively, much higher than the power density WJGL currently adopted. [131]

Table 4
the parameters for different cases.

Application	Materials	Laser Type	Average Power (W)	Nozzle Size (μm)	Water Pressure (MPa)	Repetition Frequency (kHz)	Pulse Energy (mJ)	Pulse Duration (ns)
Fuel Nozzle [123,124]	440C Stainless Steel	Nd:YAG 1064 nm	18	20	50	2	9	10–50
Aerospace [114]	Nickel Based Superalloys		10–120	50–100	10–40	6–24		100–500
Aerospace/Tools [125]	CFRP, CMC, CFRC	Green Fiber Laser	350			10–40	1–15	400–600
Semiconductor [126,127]	Gaas Wafers	Nd:YAG	19	75	20	25	2.5	450
Semiconductor [128]	Sapphire	Nd:YAG 532 Nm	5–60	40–50	10–70	6–20		80–250
Tools [125]	Ceramics and Hard Materials	Nd:YAG	5–350			5–40	7–50	80–500
Gem [129]	Natural Diamond	Nd:YAG 532 Nm	30–40	50	5–40	6	6–7	10–150

5.3. State of art application

WJGL enables the gentle cutting, grooving and dicing of sensitive materials resulting in smooth edges, high wafer fracture strength and less risk of breakage, allowing precise ablation of various semiconductor materials such as silicon (Si), gallium arsenide (GaAs), silicon carbide (SiC), low-K materials of various thicknesses. M. Gobet conducted experiments of laser scribing and grooving on SiC, thin film solar cells, edge isolation and Si wafer by green short-pulse (10 ns) and long pulse laser (350 ns). The results show that short pulse is well suited for these application with excellent kerf quality and free of chipping and burrs. [132] D. Perrottet studied the fracture strengths of GaAs, Low k wafer, SiC thin wafers diced with WJGL, conventional dry laser and conventional sawing. It was found that trenching by WJGL achieves the highest die strength, around 30–50% higher than dry laser and sawing, due to high quality of cutting edge [132,133]. M. Dushkina mentioned that dicing of GaAs wafer with WJGL is much safer than expected since water cooling keep the average temperature in the cutting point far below the level of decomposition of the material and generation of arsine gas in dangerous concentrations. [127]

The cutting of ultra-hard diamond tool materials, natural diamond, and sapphire with WJGL is showing very promising results in terms of low surface roughness and high cutting speed. G. Shi compared natural diamond cuts machined by WJGL and dry laser. The high temperature of natural diamond surfaces yielded by both laser cuttings make natural diamond changing into graphite. However, the natural diamond surface cut by WJGL only forms a thinner layer of carbon allotrope covered on the diamond surface, leading little residual stress and less micro cracks [134]. A. Richmann used WJGL to cut sapphire up to 3 mm thick with parallel walls with a roughness of < 0.5 μm and a kerf width of < 100 μm achieved. The edges at the front side exhibit high quality with a radius of curvature of less than 20 μm and without any chipping. Processing strategies are necessary to achieve thick cutting due to non-planar surfaces which lead the loss of energy on the way to the work piece and therefore interruption of the absorption and ablation process [23]. Artificial ultra-hard materials, such as polycrystalline diamond (PCD), mono-crystalline diamond (MCD), cubic boron nitride (CBN), and chemical vapor deposition diamond (CVD), are replacing tungsten carbide and ceramic composites in cutting and abrasive tools where high surface finish quality is required. Classical machining of such extreme hard materials with EDM or dry laser require important post treatment of the edges. WJGL offers important advantages in this field: the edges are perfectly rectangular, without contamination or deposit and free of heat influence. The surface quality is as good as after EDM [135].

WJGL is superior to conventional laser on machined and processed advanced composite materials like metal matrix composites (MMC) and ceramic matrix composite (CMC) due to the differences in the chemical and physical properties of the hard-ceramic components and complex mechanical structure. Experimental investigations were conducted by S Marimuthu to understand the characteristics of WJGL drilling of aluminum MMCs reinforced with silicon carbide particles. Results show both matrix and reinforcement particles are removed by the same process of cold ablation without leaving any residual melt layer within the bulk material, completely different from the millisecond laser drilling process in which the solid SiC are ejected along with the molten aluminum matrix. The hole taper and thermal damage with WJGL drilling are significantly less compared to the millisecond laser drilling process [136]. D. Sun conducted a series of experiments to evaluate the strategies on WJGL cutting of CFRP laminate. Multi-pass scanning strategy without parallel passes led a saw tooth shape on the side wall of the kerf mainly due to the flow of water. Trimming the finishing surface and the machined surface quality can be improved in last pass by optimizing the parameters [137].

Metal components also can be machined and processed by WJGL with advantages. C.A.A. Rashed and L. Romoli compared the machined surfaces of martensitic AISI 440C stainless steel fuel injector nozzles

machined by WJGL drilling, ultrafast laser drilling, and EDM micro-drilling. As a result, the efficient melt expulsion and immediate cooling of WJGL generates electro-eroded surfaces with peak to valley distances of 800 nm with a periodicity of 18 μm, much better than those by EDM. WJGL also showed finer and smaller cracks in the re-solidified surface layer than ultrafast laser drilling [123,138]. A. Richmann compared WJGL, ultrafast fast laser, and Electrical discharge machining (EDM) for cutting watch parts composed of maraging steel, stainless steel, brass and CuBe. WJGL meets the requirements of high cutting speeds with considerable low requirements on the roughness on the kerf. Also, the parallel kerf when cutting with WJGL is an advantage. All materials including toxic materials like CuBe can be cut. The heat damage of the material is supposed to be less. This comparison study shows that the WJGL is a reasonable alternative to dry laser cutting [18]. Klaus Hock compared thin metal sheet cutting with remote fiber laser and WJGL. A test pattern with complex contours was processed in stainless steel and brass sheets with thickness less than 100 μm. Results reveal that the water-jet guided system has mayor advantages in a reduced heat affected zone, dross height, kerf width and smallest possible bridges, whilst remote fiber laser shows higher cutting speed and therefore the higher productivity and lower process costs. WJGL is suitable for very thin material layers and those processes were very high quality is required [139]. Yixin Bai experimentally investigated the influence of the laser parameters and process strategy on the roughness of the kerf cut by WJGL. Single pass cutting and shorter pulse width is preferable for brass thin metal cut to achieve a low roughness. For pulse energies larger than a threshold, the roughness increases due to the heat effects occurring. A smaller overlap leads to an increase in surface roughness but lower cutting speed [83]. B. Adelmann investigated the ability of WJGL to cut thick aluminum, titanium, and steel with very high aspect ratio. The influence of average laser power, pulse repetition rate, and number of passes are studied. An increase of laser power and a decrease of repetition rate by trend lead to an increase of the cutting depth. The number of passes reveals a saturation type behavior due to the absorption of scattered laser radiation in the adjacent material of the processed workpiece. [140]

WJGL also can be used underwater instead of high pressure gas jet for cutting to remove the molten material through the kerf. S. Mullick investigated a study of a high velocity coaxial waterjet assisted underwater laser cutting process using a high power fiber laser, the results shown that less turbulence and gas bubbles are produced. [141]

5.4. Hybrid processing

Laser chemical processing (LCP) was invented by Kray and Willeke and its principle is based on waterjet guided laser in which liquid jet instead waterjet as shown in Fig. 23 [142]. LCP is commercialized by the company Synova.

Laser chemical processing (LCP) has been under development with ultra-pure water substituted by a specific chemical solution in the WJGL procedure. The liquids contain a perfluoro-carbon compound as solvent and elemental chlorine as etching agent is studied for silicon grooving. It is shown that with the addition of low-concentration chlorine, a very promising result, possibly due to a kind of tensidic effect, shows significantly higher ablation rates, whilst an about four times greater groove depth was achieved by compared to groove depths without using chlorine [143]. The liquids containing a dopant source were chosen for selective doping via the laser-induced physical and chemical interactions of the substrate and doping medium. H₃PO₄ is chosen as the doping carrier medium to fabricate high-efficiency oxide-passivated LFC solar cells exhibiting efficiencies above 20% and allow for even higher performance when smaller contact widths are used. [144] Phosphoric acid was used for n-type doping of poly-silicon thin films on glass substrates. The doping concentration and doping depth are promising for its application on poly-Si thin film solar cells [145]. LCP doping with alkaline aqueous boron solution exhibited the promising ability on p-

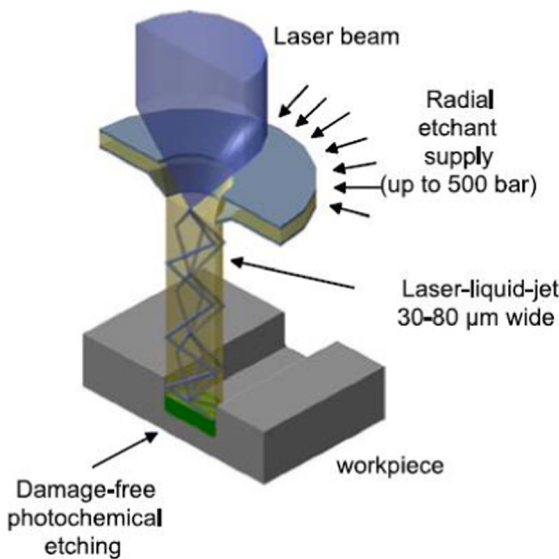


Fig. 23. Principle of Laser Chemical Processing (LCP).

type boron doping due to the lower binding energy of the containing boron complexes in contrast to the B-O complexes in boric acid and the higher solubility or amount of boron in a solvent [146].

Peeling, micro-cracks and chipping of metal or oxide layers during wafer sawing represents major issues in dicing. Wafer materials with complex layers are more prone to be broken and damaged by abrasive saw dicing processes. Synova and Disco collaborated to develop a hybrid dicing tool where dicing saw is used for bulk silicon wafer cutting and WJGL is used for surface layers, leading more accurate, tender and delicate processing. The greatly reduced mechanical stress and damage experienced by the material, results in a significantly better chip yield, whilst the reduced usage of the diamond saw blade reduces machine running costs. [147]

Modern turbine blades use exotic super-alloys, internal cooling air channels and thermal barrier coatings to survive in harsh environment. Synova and Makino collaborated on a hybrid cell to drill precision holes on turbine blades. The WJGL system cuts diffuser shapes in the coating layer and drills metering holes, whilst the EDM machines drill deep through holes. The hybrid process enables drilling holes in components already precoated with a thermal barrier, as opposed to conventional post-coating drilling processes [148].

6. Technical difficulties and the developmental trends of waterjet guided laser

(1) Finer water jet and higher power intensity laser: The diameter of the water jet will affect the cutting width and thus the cutting accuracy. The current water jet diameter can reach 20 μm. For processing, the smaller the water jet diameter, the higher the cutting accuracy, and the more difficult to stabilize the water jet. The stability and coherence length of the water jet are related to the interaction between gas and water, laser parameters, and coupling head shape. A lot of puzzles and difficulties are required to be solved in researches. With increasing of laser intensity, the nonlinear absorption of water increases which leads to energy loss. Attenuation of high power intensity laser beam in water needs attention in research.

(2) Small and deep hole drilling: The essence of the water-guided laser processing principle is to use laser to remove material. When drilling deep holes, the water is entrapped in the hole, and the residue in the hole and the turbulence of water will affect the laser propagation. At the same time, the high power density laser beam energy is greatly attenuated in water. This affects the processing speed of deep holes. Therefore, fluid parameters and processing methods in deep holes

drilling need to be studied to ensure the accuracy of processing.

7. Future directions of WJGL research

(1) Distribution of laser energy in workpiece: The water jet forms impingement jet on the surface of workpiece, and its shape affects the laser energy distribution. The laser incidence angle affects not only the coupling efficiency, but also the energy distribution in the impinging jet. The research in this respect can improve the precision of waterjet guided laser technology.

(2) Improve laser transmission efficiency: Study the attenuation law of the laser in the water and the coupling method of the laser and the water jet to reduce the attenuation energy in the water. Further attention should be paid to increasing the laser power while ensuring the beam quality.

(3) Most of works presented in waterjet guided laser technology are aimed to study laser-matter interaction and stability of waterjet. Only few researchers give insight into the interactions between the laser beam, waterjet and workpiece material. There is a need for further perfection of multi-physical modeling.

(4) Ultra-hard material processing: WJGL offers important advantages in processing hard materials, such as diamond, Sic etc. The edges are perfect, without contamination or deposit and free of heat influence. However, the application scope of waterjet guided laser cutting ultra-hard materials is relatively small, so the applications of WJGL processing superhard materials need to be concerned.

8. Conclusion

This review reports a series of literature on the topic of water-jet laser technology. It has clearly outlined the many potentials of the water-jet laser technology and demonstrated that it is undoubtedly an appropriate machining technology for various applications.

In particular, the paper discussed the hydrodynamic phenomena, mainly about waterjet stability. The cavitation zone increases the length of the reattachment and the distance from the nozzle to the hydraulic flip. Hydraulic flip is caused by cavitation and will improve the stability of water jet. Liquid jet breakup is a complex phenomenon and dependent on many intrinsic and extrinsic factors, mainly about water hydrodynamic and thermos-physical properties, ambient environment, nozzle geometry, and hydraulic parameters of pressure and flow rate.

It has clearly outlined different aspect of laser-waterjet coupling like coupling unit, parameters, loss, propagation modes and speckle etc. The absorption of the laser by the water jet is an important factor when considering how much of the original laser power is transmitted to the workpiece. The refractive index of water changes with the change of wavelength and temperature. With the increase of temperature, the refractive index of water decreases slightly. The major factors which affect transmission efficiency are wavelength of laser, focal position and numerical aperture.

The mild process and high-quality performance results enable WJGL to handle a wide range of materials, and modeling and simulation can provide appropriate assistance in understanding the physical mechanisms involved in laser ablation, particularly those related to achieving the desired ablation contours and maximum ablation depth. And ablation ability and quality, kerf size and geometry are determined by material properties of the workpiece and appropriate selection of the cutting parameters.

The motivation for studying the current status of WJGL processing extends to optimizing production and improving product range.

Declaration of Competing Interest

The authors declare that they have no known competing financial interests or personal relationships that could have appeared to influence the work reported in this paper.

Acknowledgements

This study was co-supported by the National Natural Science Foundation of China (51875558). We would like to acknowledge Technology and Hubei Key Laboratory of Ship and Marine Hydrodynamics.

References

- [1] D. Colladon, On the reflections of a ray of light inside a parabolic liquid stream, *Comptes Rendus* 15 (1842) 800–802.
- [2] J. Hecht, City of Light, Story Fiber Optics (1999).
- [3] T.H. Maiman, Stimulated optical radiation in ruby, *Nature* 187 (4736) (1960) 493–494.
- [4] E. Snitzer, Cylindrical dielectric waveguide modes, *JOSA* 51 (5) (1961) 491–498.
- [5] D.M. Roessler, Laser processing of materials for automotive applications, *Mater. Manuf. Process* 4 (3) (1989) 285–310.
- [6] Y. Doi, Laser knife, Google Patents (1987).
- [7] W.-G. Wrobel, Process for cutting a material by means of a laser beam, Google Patents (1990).
- [8] R. Sander, H. Poesl, F. Frank, P. Meister, M. Strobel, A. Spuhler, An Nd:YAG laser with a water-guided laser beam—a new transmission system, *Gastrointest. Endosc.* 34 (4) (1988) 336–338.
- [9] R.M. Pick, G.L. Powell, Laser in dentistry Soft-tissue procedures, *Dent. Clin. North Am.* 37 (2) (1993) 281–296.
- [10] B. Richerzhagen, Method and apparatus for machining material with a liquid-guided laser beam, Google Patents (1999).
- [11] A. Kruusing, Underwater and water-assisted laser processing: Part 1—general features, steam cleaning and shock processing, *Opt. Lasers Eng.* 41 (2) (2004) 307–327.
- [12] A. Kruusing, Underwater and water-assisted laser processing: Part 2—Etching, cutting and rarely used methods, *Opt. Lasers Eng.* 41 (2) (2004) 329–352.
- [13] Sugino.com, Water Beam Machine. <http://www.sugino.com/site/water-jet-and-laser-machine-e>. (Accessed 5-15 2020).
- [14] avonysis.com, Avonysis Waterjet Guided Laser. <http://avonysis.com/avonysis-waterjet-guided-laser-technology.html>. (Accessed 5-15 2020).
- [15] Laser / Water Jet Cutting System. https://www.shibuya.co.jp/en/cutting/las_lamcs.html. (Accessed 5-15 2020).
- [16] Z. Sokolowski, I. Malinowski, Perspectives of applications of micro-machining utilizing water jet guided laser, Springer, Berlin Heidelberg, Berlin, Heidelberg, 2007, pp. 365–369.
- [17] J. Battaglia, D. Perrotte, B. Richerzhagen, Damage-free micro machining using the water-jet-guided laser technology, (2005).
- [18] A. Richmann, B. Richerzhagen, Comparison study: Cutting with the laser microjet® vs. well-established and new micro-machining technologies for applications of the watch industry, *International Congress on Applications of Lasers & Electro-Optics* (1) (2014) 269–277.
- [19] J. Battaglia, D. Perrotte, R. Housh, B. Richerzhagen, Synova has re-invented the laser: No heat damage, no beam divergence, no cutting gas, no deposition, *Int. Congr. Appl. Lasers Electro-Optics 2006* (1) (2006) M905.
- [20] B. Richerzhagen, The best of both worlds—laser and water jet combined in a new process: The water jet guided laser, *Int. Congr. Appl. Lasers Electro-Optics 2001* (1) (2001) 1815–1824.
- [21] W. KrÖninger, D. Perrotte, J.-M. Buchilly, B. Richerzhagen, Stress release increases advantages of laser-microjet, *Semiconductor Int.* 28 (4) (2005), SP-4.
- [22] V.M. Tabie, M.O. Koranteng, A. Yunus, F. Kuuyine, Water-Jet Guided Laser Cutting Technology- an Overview, *Lasers Manuf. Mater. Process.* 6 (2) (2019) 189–203.
- [23] A. Richmann, Y. Kuzminykh, B. Richerzhagen, P. Hoffmann, Laser microjet® cutting of up to 3 mm thick sapphire, *Int. Congr. Appl. Lasers Electro-Optics 2014* (1) (2014) 1139–1143.
- [24] B. Richerzhagen, R. Housh, F. Wagner, J. Manley, Waterjet Guided Laser Cutting: A Powerful Hybrid Technology for Fine Cutting and Grooving, Society of Manufacturing Engineers, 2000.
- [25] Laser MicroJet® Integration Package (LMJ-iP). https://www.hasmakt.com/cms-uploads/PDF/Web_Brochure_LMJ-iP_2017.pdf. (Accessed 5-15 2020).
- [26] A.W. Momber, R. Kovacevic, *Principles of Abrasive Water Jet Machining*, Springer, London, 1998.
- [27] A. Richmann, S. Kurzen, B. Carron, B. Richerzhagen, Cutting diamond tools using the Laser MicroJet® technology on a 5-axis machine, 2015.
- [28] P. Radhakrishnan, Computer numerical control machines and computer aided manufacture, New Academic Science Ltd, 2014.
- [29] W.P. Jüptner, LIA handbook of laser materials processing, *IEEE Circuits Devices Mag.* 38 (6) (2002) 608–610.
- [30] N.B. Dahotre, S. Harimkar, *Laser Fabrication and Machining of Materials* (2008).
- [31] X. Chen, X. Li, C. Wu, Y. Ma, Y. Zhang, L. Huang, W. Liu, Optimization of Processing Parameters for Water-Jet-Assisted Laser Etching of Polycrystalline Silicon, *Appl. Sci.* 9 (9) (2019) 1882.
- [32] E.J. Weller, Nontraditional Machining Processes (1984).
- [33] G. Yang, *Laser ablation in liquids: principles and applications in the preparation of nanomaterials*, CRC Press, 2012.
- [34] J.K. Vennard, L. Robert Street, *Elementary Fluid Mech.* (1965).
- [35] S.P. Lin, K.J. Ruschak, Breakup of Liquid Sheets and Jets, *Appl. Mech. Rev.* 57 (4) (2004) B23.
- [36] L. Ting, J.B. Keller, Slender Jets and Thin Sheets with Surface Tension, *SIAM J. Appl. Math.* 50 (6) (1990) 1533–1546.
- [37] D.T. Papageorgiou, Analytical description of the breakup of liquid jets, *J. Fluid Mech.* 301 (1995) 109–132.
- [38] G. Alfonsi, Reynolds-Averaged Navier-Stokes Equations for Turbulence Modeling, *Appl. Mech. Rev.* 62 (4) (2009) 20.
- [39] M. Wei, Y. Liu, Z. Liu, T. Zhang, Investigation on the Stability of Capillary Waterjet as the Optical Waveguide Influenced by Cavitation, *2018 IEEE 8th International Conference on Underwater System Technology: Theory and Applications (USYS)*, 2018, pp. 1–5.
- [40] F. Xiao, M. Dianat, J.J. McGuirk, Large Eddy Simulation of Single Droplet and Liquid Jet Primary Breakup Using a Coupled Level Set/Volume of Fluid Method 24 (4) (2014) 281–302.
- [41] X. Jiang, G.A. Siamas, K. Jagus, T.G. Karayannidis, Physical modelling and advanced simulations of gas–liquid two-phase jet flows in atomization and sprays, *Prog. Energy Combust. Sci.* 36 (2) (2010) 131–167.
- [42] J. Shinjo, A. Umemura, Simulation of liquid jet primary breakup: Dynamics of ligament and droplet formation, *Int. J. Multiph. Flow* 36 (7) (2010) 513–532.
- [43] M. Gorokhovski, M. Herrmann, Modeling primary atomization, *Annu. Rev. Fluid Mech.* 40 (1) (2008) 343–366.
- [44] S.O. Unverdi, G. Tryggvason, A front-tracking method for viscous, incompressible, multi-fluid flows, (1992).
- [45] C.W. Hirt, B.D. Nichols, Volume of fluid /VOF/ method for the dynamics of free boundaries, *J. Comput. Phys.* 39 (1981) 201–225.
- [46] S. Osher, Fronts propagating with curvature dependent speed : Algorithms base on Hamilton-Jacobi formulations, *J. Comput. Phys.* 79 (1988).
- [47] M. Sussman, E.G. Puckett, A Coupled Level Set and Volume-of-Fluid Method for Computing 3D and Axisymmetric Incompressible Two-Phase Flows, *J. Comput. Phys.* 162 (2) (2000) 301–337.
- [48] J.W. Strutt, L. Rayleigh, On the instability of jets, *Proc. London Math. Soc* 10 (4) (1878).
- [49] C. Weber, Zum zerfall eines flüssigkeitsstrahles, *ZAMM-J. Appl. Mathem. Mech./Zeitschrift für Angewandte Mathematik und Mechanik* 11 (2) (1931) 136–154.
- [50] R.A. Castleman, The mechanism of the atomization of liquids, (1931).
- [51] G.I. Taylor, Generation of ripples by wind blowing over a viscous fluid. Reprinted in *The Scientific Papers of Sir Geoffrey Ingram Taylor*, Vol. 3, Cambridge Univ. Press, London, 1963.
- [52] G.I. Taylor, The instability of liquid surfaces when accelerated in a direction perpendicular to their planes. I, *Proc. R. Soc. Lond. A* 201 (1965) (1950) 192–196.
- [53] R.P. Fraser, P. Eisenklam, N. Dombrowski, D. Hasson, Drop formation from rapidly moving liquid sheets, *AIChE J.* 8 (5) (1962) 672–680.
- [54] R.P. Fraser, Research into the performance of atomizers for liquids, *Imp. Coll. Chem. Eng. Soc. J.* 7 (1953) 52–68.
- [55] A. Mansour, N. Chigier, Disintegration of liquid sheets, *Phys. Fluids A Fluid Dyn.* 2 (5) (1990) 706–719.
- [56] N. Chigier, Z. Farago, Morphological classification of disintegration of round liquid jets in a coaxial air stream, *Atomization Sprays* 2 (2) (1992).
- [57] Y.T. Tanasawa, On the atomization of liquid jet issuing from a cylindrical nozzle, *Technol. Rep. Tohoku Univ.* 19 (1955) 135.
- [58] H. Vahedi Tafreshi, B. Pourdeyhimi, The effects of nozzle geometry on waterjet breakup at high Reynolds numbers, *Exp. Fluids* 35 (4) (2003) 364–371.
- [59] W.H. Nurick, Orifice Cavitation and Its Effect on Spray Mixing, *J. Fluids Eng.* 98 (4) (1976) 681–687.
- [60] Fluent-Ansys, Ansys Fluent 12.0 Theory Guide, ANSYS Inc., Canonsburg, PA (2009).
- [61] H. Hiroyasu, Spray breakup mechanism from the hole-type nozzle and its applications, *Atom. Sprays* 10 (3–5) (2000) 511–527.
- [62] N. Anantharamaiah, An investigation of the influence of nozzle geometry in the hydroentangling process, (2006).
- [63] M. Arai, M. Shimizu, H. Hiroyasu, Break-up length and spray angle of high speed jet (1985) 1–10.
- [64] H. Hiroyasu, Break-up length of a liquid jet and internal flow in a nozzle (1991) 275–282.
- [65] A. Fluent, Ansys fluent theory guide, ANSYS Inc., USA 15317 (2011) 724–746.
- [66] N. Anantharamaiah, H. Vahedi Tafreshi, B. Pourdeyhimi, A study on hydroentangling waterjets and their impact forces, *Exp. Fluids* 41 (1) (2006) 103–113.
- [67] Rayleigh Lord, On the Capillary Phenomena of Jets (1879).
- [68] F. Wagner, O. Sibaily, N. Vágó, R. Romanowicz, B. Richerzhagen, The laser microjet® technology – 10 years of development, *Int. Congr. Appl. Lasers Electro-Optics 2003* (1) (2003) M401.
- [69] A.M. Sterling, C.A. Sleicher, The instability of capillary jets, *J. Fluid Mech.* 68 (3) (1975) 477–495.
- [70] S.P. Lin, R.D. Reitz, Drop and spray formation from a liquid jet, *Annu. Rev. Fluid Mech.* 30 (1) (1998) 85–105.
- [71] R.D. Reitz, N. Chigier, Regimes of jet breakup and breakup mechanisms (physical aspects), *Prog. Astronaut. Aeronaut.* 166 (1996) 109.
- [72] J.C. Lasheras, E.J. Hopfinger, Liquid jet instability and atomization in a coaxial gas stream, *Annu. Rev. Fluid Mech.* 32 (1) (2000) 275–308.
- [73] J. Mazallon, Z. Dai, G.M. Faeth, Primary breakup of nonturbulent round liquid jets in gas crossflows, *Atomization Sprays* 9 (3) (1999).
- [74] R. Cadavid, D. Wüstenberg, H. Louis, F. Pude, T. Senne, Effect of helium atmospheres on abrasive suspension water jets, *Int. J. Adv. Manuf. Technol.* 26 (11–12) (2005) 1246–1254.

- [75] Z. Wang, Investigation of the Water Guided Laser Micro-Jet Machining of, Aero Engine Components (2017).
- [76] J. Gaebelein, J. Hribar, A. Ag, Pushing the envelope of liquid-jet guided laser machining applying modern IR fiber lasers, 2019.
- [77] N. Zuckerman, N. Lior, I. Summary, Jet Impingement Heat Transfer: Physics, Correlations, and Numerical Modeling (2006).
- [78] S.H. Feng, Chuanzhen; Wang, Jun; Zhu, Hongtao, Material removal of single crystal 4H-SiC wafers in hybrid laser-waterjet micromachining process, Mater. Sci. Semicond. Process. 82 (2018) 112–125.
- [79] P. Schiebener, J. Straub, J.M.H. Levelt Sengers, J.S. Gallagher, Refractive index of water and steam as function of wavelength, temperature and density, J. Phys. Chem. Ref. Data 19 (3) (1990) 677–717.
- [80] A.N. Bashkatov, E.A. Genina, Water refractive index in dependence on temperature and wavelength: a simple approximation, Proceedings of SPIE 5068 (2003) 393–395.
- [81] P. Couty, F.R. Wagner, P.W. Hoffmann, Laser coupling with a multimode water-jet waveguide, Opt. Eng. 44 (6) (2005) 1–8.
- [82] D.S. Hobbs, B.D. Macleod, E. Sabatino, J.A. Britten, C.J. Stoltz, Contamination resistant antireflection nano-textures in fused silica for laser optics, SPIE Laser Damage (2013).
- [83] Y. Baia, A. Richmann, J. Paikb, B. Richerzhagen, Reducing the Roughness of the Kerf for Brass Sheet Cutting with the Laser MicroJet® by a Systematic Parameter Study, 2015.
- [84] F. Schmidt, H. Janssen, C. Brecher, Realization and first time operation of a high-power laser-water-jet system, (2017).
- [85] Y. Shen, Y.Q. Huang, R.F. Ye, S. Ding, L. Wang, C. Lin, Y. Gu, A New Design of The Laser-Micro Jet System, Sympos. Photon. Optoelectron. 2009 (2009) 1–4.
- [86] B. Richerzhagen, Interferometer for measuring the absolute refractive index of liquid water as a function of temperature at 1.064 μm, Appl. Opt. 35 (10) (1996) 1650–1653.
- [87] G. Stewart, Optical Waveguide Theory (1983).
- [88] N. Vágó, Á. Spiegel, P. Couty, F.R. Wagner, B. Richerzhagen, New technique for high-speed microjet breakup analysis, Exp. Fluids 35 (4) (2003) 303–309.
- [89] Y. Huang, Y. Zhao, L. Yang, J. Zhou, H. Jiao, Y. Long, Theoretical study of water jet guided laser technology based on non-uniform electric field deflection water jet, Opt. Commun. 442 (2019) 31–39.
- [90] L.J. Yang, C.Q. Li, J. Tang, Y. Wang, Y.B. Chen, Analysis on the Coupling Error of Laser and Water-Jet in Water-Jet Guided Laser Micromachining, Adv. Mater. Res. 188 (2011) 190–194.
- [91] L. Li, L.-J. Yang, Y. Wang, B. Liu, Z. Wang, Laser and water-jet fiber coupling technology for water-jet guided laser micromachining, Guangxue Jingmi Gongcheng (Optics Precis. Eng.) 16 (9) (2008) 1614–1621.
- [92] P. Couty, A. Spiegel, N. Vágó, B.I. Ugurtas, P. Hoffmann, Laser-induced break-up of water jet waveguide, Exp. Fluids 36 (6) (2004) 919–927.
- [93] B. Richerzhagen, G.P. Delacretaz, R.-P. Salathe, Complete model to simulate the thermal defocusing of a laser beam focused in water, Opt. Eng. 35 (7) (1996), 2058–2066, 9.
- [94] Y. Qiu, G. Zhu, X. Zhu, Y. Chen, C. Zhu, Influence of Water-Jet Waveguide with Turbulent Surface on the Optical Transmission Losses, Zhongguo Jiguang (Chin. J. Lasers) 43 (1) (2016) 0116003.
- [95] A. Vogel, W. Lauterborn, R. Timm, Optical and acoustic investigations of the dynamics of laser-produced cavitation bubbles near a solid boundary, J. Fluid Mech. 206 (1989).
- [96] C. Brecher, H. Janssen, M. Eckert, F. Schmidt, Thermal Investigation of Interaction between High-power CW-laser Radiation and a Water-jet, Physics Procedia 83 (2016) 317–327.
- [97] 李清, 水中湍流对光传输影响的光线追迹算法的研究, 华中科技大学, 2011.
- [98] M. Young, Optics and lasers: Including fibers and optical waveguides, 1986.
- [99] D. Malacara, B.J. Thompson, Handbook of optical engineering, Marcel Dekker, New York, 2001.
- [100] G.C. Papen, G.M. Murphy, Modal Noise in Multimode Fibers under Restricted Launch Conditions, J. Lightwave Technol. 17 (5) (1999) 817.
- [101] T.A. Mai, Fundamental and Beam Propagation Behaviour of a MicroJet and Recent Applications using Laser MicroJet Technology (2007) 1–5.
- [102] A. Spiegel, N. Vago, F.R. Wagner, High efficiency Raman scattering in micrometer-sized water jets, Opt. Eng. 43 (2) (2004) 450–454.
- [103] M. Maier, W. Kaiser, Threshold of stimulated Raman scattering in liquids and self-focusing of laser beams, Phys. Lett. 21 (5) (1966) 529–530.
- [104] J.S. Bartlett, K.J. Voss, S. Sathyendranath, A. Vodacek, Raman scattering by pure water and seawater, Appl. Opt. 37 (15) (1998) 3324–3332.
- [105] V.A. Babenko, N.F. Bunkin, A.A. Sychev, Effect of an optical breakdown on the stimulated raman scattering in water in the field of picosecond laser pulses, J. Exp. Theor. Phys. 128 (5) (2019) 664–671.
- [106] U. Eppelt, Modeling and simulation of water jet-guided laser radiation, 2014, p. 55.
- [107] A. Pauchard, M. Gobet, F. Juvet, A. Schreiner, Metal and stent cutting using water jet-guided laser technology, Laser Inst. Am. (2010) 1139–1145.
- [108] A. Pauchard, N. Vago, B. Richerzhagen, Experimental micromachining results using a UV laser with the laser microjet®, Pacific Int. Conf. Appl. Lasers Optics 2008 (1) (2008) 709–714.
- [109] D. Perrottet, S. Amorosi, B. Richerzhagen, Water-jet guided fiber lasers for mask cutting, Int. Congr. Appl. Lasers Electro-Optics 2005 (1) (2005) M206.
- [110] A. Gropp, J. Hutfless, S. Schuberth, M. Geiger, Laser beam cutting, Opt. Quant. Electron. 27 (12) (1995) 1257–1271.
- [111] S. Nisar, M.A. Sheikh, L. Li, S. Safdar, Effect of thermal stresses on chip-free diode laser cutting of glass, Opt. Laser Technol. 41 (3) (2009) 318–327.
- [112] J.R. Lawrence, Advances in laser materials processing: technology, research and applications, Woodhead Publishing, 2017.
- [113] J.A. Porter, Y.A. Louhisalmi, J.A. Karjalainen, S. Füger, Cutting thin sheet metal with a water jet guided laser using various cutting distances, feed speeds and angles of incidence, Int. J. Adv. Manuf. Technol. 33 (9) (2007) 961–967.
- [114] J. Diboine, R. Martin, F. Bruckert, H. Diehl, B. Richerzhagen, Towards near-net shape micro-machining of aerospace materials by means of a water jet-guided laser beam, 2017.
- [115] M. Stafe, A. Marcu, N.N. Puscas, SpringerLink, Pulsed Laser Ablation of Solids: Basics, Theory and Applications, Springer, Berlin Heidelberg, Berlin, Heidelberg, 2014.
- [116] A.K. Dubey, V. Yadava, Optimization of kerf quality during pulsed laser cutting of aluminium alloy sheet, J. Mater. Process. Technol. 204 (1–3) (2008) 412–418.
- [117] M.J. Hsu, P.A. Molian, Off-axial, gas-jet-assisted, laser cutting of 6.35-mm thick stainless steel, (1995).
- [118] P.M. Ilavarasan, P.A. Molian, Laser cutting of thick sectioned steels using gas flow impingement on the erosion front, J. Laser Appl. 7 (4) (1995) 199–209.
- [119] C.F. Li, D.B. Johnson, R. Kovacevic, Modelling of heat transfer in waterjet guided laser drilling of silicon, Proc. Inst. Mech. Eng., Part B: J. Eng. Manuf. 217 (5) (2003) 583–600.
- [120] H. Zhu, J. Wang, P. Yao, C. Huang, Heat transfer and material ablation in hybrid laser-waterjet microgrooving of single crystalline germanium, Int. J. Mach. Tools Manuf. 116 (2017) 25–39.
- [121] C.F. Li, D.B. Johnson, R. Kovacevic, Modeling of waterjet guided laser grooving of silicon, Int. J. Mach. Tools Manuf. 43 (9) (2003) 925–936.
- [122] Y.K. Madhukar, S. Mullick, A.K. Nath, A study on co-axial water-jet assisted fiber laser grooving of silicon, J. Mater. Process. Technol. 227 (2016) 200–215.
- [123] L. Romoli, G. Lovicu, C.A.A. Rashed, G. Dini, M. De Sanctis, M. Fiaschi, Microstructural Changes Induced by Ultrashort Pulsed Lasers in Microdrilling of Fuel Nozzles, Procedia CIRP 33 (2015) 508–513.
- [124] C.A.A. Rashed, G. Dini, L. Romoli, Laser Based Processes in, Modern Production System, 2015.
- [125] H. Diehl, J. Diboine, R. Martin, B. Richerzhagen, Application of 400-W laser MicroJet for high-throughput and low-impact micro-structuring of aerospace and tooling industry parts (Conference Presentation), SPIE2018.
- [126] N.M. Dushkina, F.R. Wagner, C. Boillat, J.-M. Buchilly, B. Richerzhagen, Water jet guided laser versus saw dicing, Proceedings of SPIE, the International Society for Optical Engineering Proceedings of SPIE, the International Society for Optical Engineering SPIE-4977 (2003) 75–85.
- [127] N.M. Dushkina, B. Richerzhagen, Dicing of gallium arsenide (GaAs) wafers with the laser MicroJet® challenges, improvements and safety issues, Laser Institute of America (2002), 851160.
- [128] T. Nilsson, F. Wagner, R. Housh, B. Richerzhagen, Scribing of GaN wafer for white LED by water-jet-guided laser, SPIE2004.
- [129] Diamond Cutting Systems. <https://www.synova.ch/products/diamond-cutting-systems/item/14-dcs-150.html>. (Accessed 5-24 2020).
- [130] W. Charee, V. Tangwarodomnukun, Dynamic features of bubble induced by a nanosecond pulse laser in still and flowing water, Opt. Laser Technol. 100 (2018) 230–243.
- [131] L. Berthe, R. Fabbro, P. Peyre, E. Bartnicki, Wavelength dependent of laser shock-wave generation in the water-confinement regime, J. Appl. Phys. 85 (11) (1999) 7552–7555.
- [132] M. Gobet, S. Obi, M. Pavius, M. Takano, N. Vago, K. Lee, Y. Kozuki, A. Pauchard, Implementation of Short-Pulse Lasers for Wafer Scribing and Grooving Applications, J. Laser Micro Nanoeng. 5 (1) (2010) 16–20.
- [133] D. Perrottet, R. Housh, B. Richerzhagen, J. Manley, Heat damage-free laser-microjet cutting achieves highest die fracture strength, Proc. SPIE SPIE-5713 (2005) 285–292.
- [134] S. GuangFeng, H. DongDong, W. Shukun, Z. Keke, Analysis and Evaluation of Natural Diamond Cut by Water Jet - guided Laser, 4th Annual International Conference on Material Engineering and Application (ICMEA 2017), Atlantis Press, 2018.
- [135] C.E. Peter J Heath PhD, MIM, The water jet laser: for cutting single crystal diamond, CVD diamond and other ultra-hard materials, 6th ZISC Conference, Synova S.A. Switzerland, 2013.
- [136] S. Marimuthu, B. Dunleavy, Y. Liu, B. Smith, A. Kiely, M. Antar, Water-jet guided laser drilling of SiC reinforced aluminium metal matrix composites, J. Compos. Mater. 53 (26–27) (2019) 3787–3796.
- [137] D. Sun, F. Han, W. Ying, The experimental investigation of water jet-guided laser cutting of CFRP, Int. J. Adv. Manuf. Technol. (2019).
- [138] C.A.A. Rashed, L. Romoli, F. Tantussi, F. Fusco, M. Burgener, G. Cusanelli, M. Allegrini, G. Dini, Water jet guided laser as an alternative to EDM for micro-drilling of fuel injector nozzles: A comparison of machined surfaces, J. Manuf. Processes 15 (4) (2013) 524–532.
- [139] K. Hock, B. Adelmann, R. Hellmann, Comparative study of remote fiber laser and water-jet guided laser cutting of thin metal sheets, Physics Procedia 39 (2012) 225–231.
- [140] B. Adelmann, C. Ngo, R. Hellmann, High aspect ratio cutting of metals using water jet guided laser, Int. J. Adv. Manuf. Technol. 80 (9) (2015) 2053–2060.
- [141] S. Mullick, Y.K. Madhukar, S. Roy, S. Kumar, D.K. Shukla, A.K. Nath, Development and parametric study of a water-jet assisted underwater laser cutting process, Int. J. Mach. Tools Manuf. 68 (2013) 48–55.
- [142] D. Kray, A. Fell, S. Hopman, K. Mayer, G.P. Willeke, S.W. Glunz, Laser Chemical Processing (LCP)—A versatile tool for microstructuring applications, Appl. Phys. A 93 (1) (2008) 99.

- [143] S. Hopman, S. Hopman, K. Mayer, K. Mayer, A. Fell, A. Fell, M. Mesec, M. Mesec, F. Granek, F. Granek, Laser cutting of silicon with the liquid jet guided laser using a chlorine-containing jet media, *Appl. Phys. A* 102 (3) (2011) 621–627.
- [144] D. Kray, M. Aleman, A. Fell, S. Hopman, K. Mayer, M. Mesec, R. Muller, G.P. Willeke, S.W. Glunz, B. Bitnar, D. Neuhaus, R. Ludemann, T. Schlenker, D. Manz, A. Bentzen, E. Sauar, A. Pauchard, B. Richerzhagen, Laser-doped silicon solar cells by Laser Chemical Processing (LCP) exceeding 20% efficiency, 2008 33rd IEEE Photovoltaic Specialists Conference, 2008, pp. 1-3.
- [145] S. Virasawmy, N. Palina, S. Chakraborty, P.I. Widenborg, B. Hoex, A.G. Aberle, Laser chemical processing (LCP) of poly-silicon thin film on glass substrates, *Energy Procedia* 33 (2013) 137–142.
- [146] S. Kluska, A. Rodofili, K. Mayer, C. Fleischmann, F. Granek, S.W. Glunz, Analysis of local boron dopings formed with LCP (2010) 1405–1409.
- [147] B. Richerzhagen, M. Plankenstein, N. Kling, K. Stay, A. Brulé, Saw + LMJ: a hybrid semiconductor dicing solution, SPIE2008.
- [148] Synova, Hybrid cell for turbine blade hole drilling, 2016.